

## Evolution of A Peculiar Type Ibn Supernova SN 2019wep

ANJASHA GANGOPADHYAY,<sup>1,2</sup> KUNTAL MISRA,<sup>2</sup> GRIFFIN HOSSEINZADEH,<sup>3</sup> IAIR ARCAVI,<sup>4,5</sup> CRAIG PELLEGRINO,<sup>6,7</sup>  
XIAOFENG WANG,<sup>8,9</sup> D. ANDREW HOWELL,<sup>6,7</sup> JAMISON BURKE,<sup>6,7</sup> JUJIA ZHANG,<sup>10,11</sup> KOJI KAWABATA,<sup>1</sup>  
MRIDWEEKA SINGH,<sup>12,13</sup> RAYA DASTIDAR,<sup>14</sup> DAICHI HIRAMATSU,<sup>6,7</sup> CURTIS MCCULLY,<sup>6,7</sup> JUN MO,<sup>8</sup> ZHIHAO CHEN,<sup>8</sup> AND  
DANFENG XIANG<sup>8</sup>

<sup>1</sup>*Hiroshima Astrophysical Science Centre, Hiroshima University, 1-3-1 Kagamiyama, Higashi-Hiroshima, Hiroshima 739-8526, Japan*

<sup>2</sup>*Aryabhata Research Institute of observational sciencES, Manora Peak, Nainital 263 002 India*

<sup>3</sup>*Steward Observatory, University of Arizona, 933 North Cherry Avenue, Tucson, AZ 85721, USA*

<sup>4</sup>*The School of Physics and Astronomy, Tel Aviv University, Tel Aviv 69978, Israel*

<sup>5</sup>*CIFAR Azrieli Global Scholars program, CIFAR, Toronto, Canada*

<sup>6</sup>*Las Cumbres Observatory, 6740 Cortona Drive Suite 102, Goleta, CA, 93117-5575 USA*

<sup>7</sup>*Department of Physics, University of California, Santa Barbara, CA 93106-9530, USA*

<sup>8</sup>*Physics Department and Tsinghua Center for Astrophysics, Tsinghua University, China*

<sup>9</sup>*Beijing Planetarium, Beijing Academy of Sciences, Beijing, 100044*

<sup>10</sup>*Yunnan Astronomical Observatory of China, Chinese Academy of Sciences, Kunming, 650216, China*

<sup>11</sup>*Key Laboratory for the Structure and Evolution of Celestial Objects, CAS, Kunming 650216, China*

<sup>12</sup>*Indian Institute of Astrophysics, 2nd Block, 100 Feet Rd, Koramangala, Bengaluru, Karnataka, India 560034*

<sup>13</sup>*Korea Astronomy and Space Science Institute, 776 Daedeokdae-ro, Yuseong-gu, Daejeon 34055, Republic of Korea*

<sup>14</sup>*Millennium Institute of Astrophysics, Nuncio Monsenor S3tero Sanz 100, Providencia, Santiago, 8320000 Chile*

### ABSTRACT

We present a high-cadence short term photometric and spectroscopic monitoring campaign of a type Ibn SN 2019wep, which is one of the rare SN Ibn after SNe 2010al and 2019uo to display signatures of flash ionization (He II, C III, N III). We compare the decline rates and rise time of SN 2019wep with other SNe Ibn and fast transients. The post-peak decline in all bands ( $0.1 \text{ mag d}^{-1}$ ) are consistent with SNe Ibn but less than the fast transients. On the other hand, the  $\Delta m_{15}$  values are slightly lower than the average values for SNe Ibn but consistent with the fast transients. The rise time is typically shorter than SNe Ibn but longer than fast transients. SN 2019wep lies at the fainter end of SNe Ibn but possesses an average luminosity amongst the fast transients sample. The peculiar color evolution places it between SNe Ib and the most extreme SNe Ibn. The bolometric light curve modelling shows resemblance with SN 2019uo with ejecta masses consistent with SNe Ib. SN 2019wep belongs to the ‘‘P cygni’’ sub-class of SNe Ibn and shows faster evolution in line velocities as compared to the ‘‘emission’’ sub-class. The post-maximum spectra show close resemblance with ASASSN-15ed hinting it to be of SN Ib nature. The low He I CSM velocities and residual H $\alpha$  further justifies it and gives evidence of an intermittent progenitor between WR and LBV star.

*Keywords:* supernovae: general – supernovae: individual: SN 2019wep – galaxies: individual: – techniques: photometric – techniques: spectroscopic

### 1. INTRODUCTION

Type Ibn Supernovae (hereafter SNe Ibn) are a rare class of core-collapse SNe (CCSNe) undergoing interaction with hydrogen poor circumstellar medium (CSM). Interaction, in general, produces narrow emission lines

— broader than H II regions but narrower than the lines arising from the outer ejecta of the SN (Pastorello et al. 2007). However, in some cases interaction happens below the photosphere without any observable narrow emission lines (e.g. Morozova et al. 2017; Andrews & Smith 2018). SNe Ibn are characterised by narrow lines of He ( $\sim 2000 \text{ km s}^{-1}$ ) in their spectra and was introduced with the discovery of SN 2006jc (Pastorello et al. 2007). This is defined in analogy with SNe IIn, which

show narrow H features (Schlegel 1990). SNe that are embedded in dense CSM may also show short-lived narrow high ionization emission lines (at  $\leq 10$  days) owing to the recombination of the CSM following the shock breakout flash or through interaction of the SN ejecta with nearby CSM. These features are known as “flash features” (e.g. Gal-Yam et al. 2014; Gal-Yam 2019).

Unlike the light curves of SNe IIn which show great photometric diversity (Nyholm et al. 2020), SNe Ibn light curves (though small in number as only less than 40 SNe Ibn are known till date (Hossein-zadeh et al. 2019)) are surprisingly homogeneous with a uniform light curve shape and decay rates of  $0.05\text{--}0.15 \text{ mag d}^{-1}$  (Hossein-zadeh et al. 2017). They typically rise within a timescale of  $\leq 15$  days and reach a peak absolute magnitude of  $M_R = -19 \text{ mag}$  (Hossein-zadeh et al. 2017), with exceptions like ASASSN-14ms which has a peak luminosity of  $M_V \sim -20.5 \text{ mag}$ , lying between normal SNe Ibn and superluminous SNe (Wang et al. 2021). Pastorello et al. (2016), however, highlighted the existence of many outliers in the SN Ibn group which are slow decliners, for example, OGLE-2012-SN-006 (Pastorello et al. 2015a) and SN 2010al (Pastorello et al. 2015b). The fast-rising and decaying nature of SNe Ibn enables their comparison with the fast transients (Drout et al. (2014); Arcavi et al. (2016); Pellegrino et al. (2021)) which may hint toward their similar origin. The light curves of Stripped envelope (SESNe; typically Ibs) are in general powered by radioactivity but in the case of SNe Ibn the light curves are too steep to reconcile for the amount of  $^{56}\text{Ni}$  contributing to the radioactive luminosity (Moriya & Maeda 2016). Instead, a combination of Ni-decay and CSM interaction are required to reproduce the light curve (Karamehmetoglu et al. 2019; Wang & Li 2019; Gangopadhyay et al. 2020a).

In the past few years, one of the most unsettling question has been regarding the progenitors giving rise to SNe Ibn explosions. The homogeneity of the light curves does not necessarily imply the homogeneity of the progenitors, which are largely dependent on the CSM configuration. Unlike SNe IIn where some have been linked to H-rich luminous blue variable (LBV) stars (e.g., Gal-Yam & Leonard (2009); Smith et al. (2010)), there have been no direct detection of SNe Ibn progenitors to date. There are two precursor detections of massive SN Ibn progenitors – the luminous outburst of the prototypical SN Ibn 2006jc, observed two years before the explosion (Foley et al. 2007; Pastorello et al. 2007; Smith et al. 2008) and the other for SN 2019uo where precursor starts  $\sim 340$  days before the explosion and is observed over 35 days (Strotjohann et al. 2021). The progenitor of SN 2006jc is believed to be a massive

star with remaining LBV properties (Pastorello et al. 2007). The stripping of the outer envelope can occur also from the massive binaries (Foley et al. 2007). Strotjohann et al. (2021) suggests that the progenitors could be Wolf-Rayet (WR) stars that have shed their hydrogen envelopes or massive stars that are stripped by a binary partner. Recent evidence of a low mass progenitor host has been proposed for PS1-12sk, which occurred in a non-star forming galaxy (Sanders et al. 2013; Hossein-zadeh et al. 2019). Based on the late time UV/Optical *HST* images, an interacting binary progenitor scenario was inferred for SNe 2006jc and 2015G (Sun et al. 2020).

### Discovery:

SNe Ibn 2019wep was discovered on 2019 December 07.96979 UT by Xing Gao (Zhang et al. 2019a) in Xingming Observatory Sky Survey (C42) images at an unfiltered mag of  $\sim 18.2$  which was estimated by several 40 sec survey images. The SN was located at R.A. =  $11^{\text{h}}04^{\text{m}}36.99^{\text{s}}$ , Dec =  $+45^{\circ}58'39''.5$  (equinox J2000.0) (Mao et al. 2019) which is about  $2''.6$  east and  $27''.6$  south of the center of the host galaxy PGC33464. Zhang et al. (2019b) obtained the classification spectrum of SN 2019wep with the 2.4 m Li-Jiang Telescope (LJT+YFOSC) of Yunnan Observatories, China. The spectrum depicted a blue continuum and highly ionized “flash features” of He II, H I and C IV. This spectrum matches with that of a young SN II with signatures of interaction. Another spectrum taken a few days later shows evidence of narrow P cygni He I features classifying it as a SN Ibn. SN 2019wep is one of the rare SNe Ibn to show signatures of flash ionisation after SNe 2019uo and 2010al.

### Estimation of explosion epoch:

Mao et al. (2019) reported the non-detection of a source in archival images of Xingming Observatory Sky Survey (C42) on 2019-05-30 (limiting mag 19.0) while the Zwicky Transient Facility (ZTF<sup>1</sup>) reported a last non-detection of the source on 2019-11-25 (MJD 58812) in *r*-band at a limiting magnitude of 19.89 mag. Four pre-maximum unfiltered data points of SN 2019wep are available in TNS<sup>2</sup> which match well with our *V*-band data. We combine the unfiltered magnitudes with our *V*-band data (since the passbands are close) and perform a parabolic fit on the combined light curve of SN 2019wep. The magnitudes are converted to flux and the fit is performed using the data up to  $\sim 6$  days after the

<sup>1</sup> <https://www.wis-tns.org/object/2019wep>; Bellm 2014; Bellm et al. 2019

<sup>2</sup> <https://www.wis-tns.org/object/2019wep>

discovery. The best-fit coefficients are used to find the roots of the equation, i.e., the value of time for which the flux equals zero. This gives the explosion epoch to be  $\text{MJD } 58824.5 \pm 2$ . The error is estimated from the fitting error associated with the data.

### Distance and Extinction:

Adopting  $H_0 = 73 \text{ km s}^{-1} \text{ Mpc}^{-1}$ ,  $\Omega_{\text{matter}}=0.27$  and  $\Omega_{\text{vacuum}}=0.73$ , we obtain a luminosity distance of 108.3 Mpc (corresponding to a redshift  $z = 0.025$ <sup>3</sup>) for SN 2019wep. The Milky Way extinction along the line of sight of SN 2019wep is  $A_V = 0.031 \text{ mag}$  (Schlafly & Finkbeiner 2011). For estimating the extinction due to the host galaxy, we estimate equivalent widths of the Na ID line in the three spectra of SN 2019wep taken on 2019-12-16, 2019-12-19 and 2019-12-24. Using the formulation by Munari & Zwitter (1997) and Poznanski et al. (2012), we estimate host galaxy  $A_V = 0.0328 \text{ mag}$ . The estimated extinction results in matching the  $(B-V)$  colors of SN 2019wep in close agreement with that of SNe 2010al and 2019uo. Thus, we adopt a total  $A_V = 0.0638 \text{ mag}$ . We use these values of distance and extinction throughout the paper.

In this paper we aim to investigate the photometric and spectroscopic evolution of the peculiar SN Ibn 2019wep which not only showed signatures of flash ionisation but also shows some similarities with SN Ib at late phases. In Section 2, we discuss the procedure of photometric and spectroscopic data reduction. In Section 3, the photometric evolution of SN 2019wep is studied and compared with other SNe Ibn and fast transients. In Section 4, we discuss the interpretation of the observed spectral features including the late-time distinct P cygni features and unique  $H\alpha$  behavior. Our conclusions are given in Section 5.

## 2. DATA ACQUISITION AND REDUCTION

We observed SN 2019wep with the 2m Las Cumbres Observatory (LCO) telescopes in the  $UBVgri$  filters from  $\sim 3$  to 98 days after explosion under the Global Supernovae Project (GSP) program. The photometric observations in  $UBVRI/ugri$  were also taken with the 0.8m Tsinghua-NAOC Telescope (TNT; Huang et al. 2012), Xinglong Observatory, China. Image subtraction was done using High Order Transform of PSF ANd Template Subtraction<sup>4</sup>. The instrumental magnitudes were estimated using DAOPHOT<sup>5</sup>. The LCO image subtrac-

tion and photometry were done with `lcogtsnpipe`<sup>6</sup> (see Valenti et al. 2011, 2016). The instrumental SN magnitudes in  $gri$  bands and  $UBV$  bands were calibrated with respect to the Sloan Digital Sky Survey (SDSS) catalog and Landolt standard fields respectively.

The photometry of SN 2019wep is presented in Table 1.

The spectroscopic observations of SN 2019wep were taken at 9 epochs spanning up to  $\sim 22$  days after explosion with the 2.0m FTN and FTS telescopes of LCO and 2.4m LJT of Yunnan Observatories, China. The 1D wavelength- and flux-calibrated spectra were extracted using the `floydsspec` pipeline<sup>7</sup> (Valenti et al. 2014) for the LCO data. Spectroscopic data of the LJT telescope was reduced using the APALL task in IRAF<sup>8</sup> followed by wavelength and flux calibration. The slit loss corrections were done by scaling the spectra to the photometry. Finally, the spectra were corrected for the heliocentric redshift of the host galaxy. The log of spectroscopic observations is given in Table 2.

## 3. PHOTOMETRIC EVOLUTION OF SN 2019WEP

The multi-band light curve evolution of SN 2019wep is shown in Figure 1. Even though our observations were unable to trace the light curve maximum, four pre-maximum unfiltered data points were reported in TNS which we combine with our  $V$ -band data to perform a polynomial fit on the early data upto 8 days. A derivative of the flux values tending to zero is used to estimate the light curve maximum which occurs at  $\text{MJD } 58828.5 \pm 2$  days. The error in the obtained values is the fitting error associated with the light curve. The maximum magnitude in  $V$ -band is estimated by fitting a cubic spline function in the light curve data upto  $\sim 10$  days. This results in a peak absolute magnitude of  $M_V = -18.26 \pm 0.20 \text{ mag}$  where the estimated error accounts for the contribution of error in magnitude, redshift and interpolation errors. Even though most of the SNe Ibn have covered the  $r$ -band maximum, which is also the case of our comparison sample, we use days since  $V$ -maximum as a reference epoch throughout the study because of a better sampling in  $V$ -band.

For estimating the peak absolute magnitude in  $r$ - and  $i$ -bands, we select the first 30 days phase bin and perform a linear fit on the light curve as suggested by Hosseinzadeh et al. (2017) where the intercept gives a measure of the peak absolute magnitude. The peak absolute magnitudes for SN 2019wep are estimated to be  $M_r = -$

<sup>3</sup> [https://ned.ipac.caltech.edu/byname?objname=PGC33464&hconst=73&omegam=0.27&omegav=0.73&corr\\_z=4](https://ned.ipac.caltech.edu/byname?objname=PGC33464&hconst=73&omegam=0.27&omegav=0.73&corr_z=4)

<sup>4</sup> <https://github.com/abecker/hotpants>

<sup>5</sup> Dominion Astrophysical Observatory Photometry

<sup>6</sup> <https://github.com/svalenti/lcogtsnpipe>

<sup>7</sup> <https://github.com/svalenti/FLOYDSpipeline>

<sup>8</sup> Image Reduction and Analysis Facility

**Table 1.** Photometry of SN 2019wep. The phase is measured with respect to  $V$ -max ( $MJD_{max}=58828.5$ ).

Date (yyyy-mm-dd)	JD (2400000+)	Phase (day)	$U$ (mag)	$B$ (mag)	$g$ (mag)	$V$ (mag)	$r$ (mag)	$i$ (mag)	Telescope
2019-12-12	58829.35	0.85	—	17.19±0.03	17.11±0.03	17.29±0.03	17.42±0.10	—	LCO
2019-12-12	58829.35	0.85	—	17.20±0.03	17.18±0.04	17.38±0.04	—	—	LCO
2019-12-13	58830.41	1.91	16.49±0.03	17.38±0.02	17.35±0.03	17.41±0.03	17.48±0.03	17.91±0.07	LCO
2019-12-13	58830.41	1.91	16.45±0.04	17.35±0.03	17.28±0.02	17.43±0.03	17.57±0.03	17.75±0.07	LCO
2019-12-15	58832.36	3.86	16.86±0.04	17.48±0.03	17.36±0.03	17.59±0.04	17.62±0.03	17.68±0.05	LCO
2019-12-15	58832.37	3.86	16.85±0.05	17.56±0.03	17.28±0.03	—	17.59±0.03	17.63±0.05	LCO
2019-12-18	58835.35	6.85	17.33±0.05	18.05±0.03	17.84±0.02	17.93±0.03	17.88±0.03	18.02±0.03	LCO
2019-12-18	58835.35	6.85	—	18.06±0.03	17.83±0.02	17.93±0.04	17.86±0.03	18.05±0.03	LCO
2019-12-18	58835.73	7.25	—	18.34±0.03	18.18±0.03	17.93±0.05	18.06±0.02	18.05±0.03	TNT
2019-12-19	58836.36	7.86	17.63±0.03	18.10±0.02	17.94±0.01	17.97±0.03	17.89±0.02	17.97±0.03	LCO
2019-12-19	58836.37	7.87	17.49±0.03	18.13±0.02	17.95±0.01	17.98±0.03	17.88±0.02	18.07±0.03	LCO
2019-12-21	58838.33	9.83	17.74±0.04	18.43±0.03	18.13±0.01	18.16±0.03	18.03±0.02	18.12±0.03	LCO
2019-12-21	58838.34	9.84	17.80±0.04	18.35±0.02	18.14±0.01	18.11±0.03	18.06±0.02	18.18±0.04	LCO
2019-12-22	58839.47	10.97	18.01±0.03	18.64±0.02	18.33±0.01	18.27±0.02	18.14±0.02	18.23±0.03	LCO
2019-12-22	58839.48	10.98	18.02±0.03	18.62±0.02	18.36±0.01	18.31±0.02	—	18.23±0.02	LCO
2019-12-24	58841.44	13.04	18.45±0.10	18.75±0.03	18.55±0.04	18.44±0.06	18.27±0.04	18.21±0.07	LCO
2019-12-24	58841.44	13.04	18.37±0.08	—	18.60±0.03	18.34±0.05	18.19±0.04	18.33±0.08	LCO
2019-12-27	58844.37	15.87	18.98±0.06	19.27±0.04	18.98±0.02	18.67±0.03	18.56±0.03	18.55±0.04	LCO
2019-12-27	58844.37	15.87	19.01±0.06	19.29±0.04	18.99±0.02	18.70±0.03	18.49±0.02	18.59±0.04	LCO
2019-12-27	58844.78	16.28	—	19.30±0.09	19.00±0.05	18.71±0.04	18.50±0.03	18.51±0.03	TNT
2019-12-28	58845.80	17.30	—	19.37±0.03	19.11±0.02	18.77±0.03	18.61±0.02	18.52±0.09	TNT
2019-12-29	58846.81	18.31	—	19.47±0.05	19.28±0.03	18.86±0.06	18.81±0.06	18.91±0.09	TNT
2019-12-30	58847.78	19.28	—	19.57±0.05	19.47±0.07	19.05±0.09	18.95±0.09	—	TNT
2020-01-01	58849.82	21.32	—	20.07±0.09	19.87±0.07	19.07±0.05	19.10±0.09	18.86±0.05	TNT
2020-01-02	58850.47	21.97	20.32±0.24	20.42±0.08	20.10±0.05	19.65±0.08	19.31±0.07	19.49±0.13	LCO
2020-01-02	58850.47	21.97	20.12±0.23	20.43±0.10	20.09±0.05	19.64±0.07	19.29±0.06	—	LCO
2020-01-02	58850.75	22.25	—	20.57±0.99	18.89±0.05	19.48±0.05	19.18±0.04	19.29±0.04	TNT
2020-01-03	58851.78	23.28	—	20.39±0.08	20.09±0.05	19.59±0.05	19.29±0.03	18.97±0.04	TNT
2020-01-04	58852.76	24.26	—	20.57±0.99	20.09±0.05	19.59±0.05	19.40±0.04	19.11±0.07	TNT
2020-01-05	58853.30	24.80	20.04±0.27	20.68±0.22	20.52±0.14	19.86±0.12	19.60±0.09	19.38±0.09	LCO
2020-01-05	58853.30	24.80	20.40±0.32	—	—	19.89±0.13	19.51±0.09	19.35±0.08	LCO
2020-01-06	58854.28	25.78	—	20.62±0.22	20.65±0.19	20.06±0.14	19.48±0.10	19.48±0.24	LCO
2020-01-06	58854.28	25.78	—	20.41±0.22	—	19.95±0.13	19.41±0.08	20.53±0.15	LCO
2020-01-14	58862.44	33.94	—	20.73±0.24	—	20.63±0.20	19.47±0.16	—	LCO
2020-01-14	58862.46	33.94	—	—	—	20.32±0.17	19.96±0.21	—	LCO
2020-01-18	58866.44	37.94	—	21.49±0.24	21.51±0.17	20.63±0.16	20.01±0.09	19.88±0.11	LCO
2020-01-18	58866.44	37.94	—	21.28±0.21	21.10±0.12	20.53±0.13	20.08±0.09	19.88±0.11	LCO
2020-01-24	58872.48	43.98	—	21.34±0.18	21.27±0.10	21.28±0.14	20.15±0.08	19.91±0.11	LCO
2020-01-24	58872.49	43.99	—	21.48±0.25	21.28±0.11	20.89±0.12	20.18±0.07	19.94±0.11	LCO
2020-01-28	58876.43	47.93	—	21.66±0.33	21.47±0.16	20.79±0.16	20.34±0.12	20.31±0.16	LCO
2020-01-28	58876.44	47.94	—	21.84±0.28	21.66±0.24	20.77±0.28	20.29±0.08	—	LCO
2020-01-28	58876.48	47.98	—	21.80±0.33	—	20.76±0.13	—	—	LCO
2020-01-28	58876.48	47.98	—	21.37±0.23	—	20.84±0.17	—	—	LCO
2020-02-01	58880.47	51.97	—	21.39±0.24	21.43±0.12	20.66±0.12	20.39±0.10	20.20±0.13	LCO
2020-02-01	58880.48	51.98	—	21.52±0.24	21.56±0.16	20.81±0.16	20.42±0.11	20.33±0.15	LCO
2020-02-08	58887.41	58.91	—	21.51±0.53	21.34±0.28	21.21±0.49	20.34±0.19	20.38±0.25	LCO
2020-02-08	58887.41	58.93	—	—	21.88±0.42	20.67±0.34	21.57±0.44	21.76±0.24	LCO
2020-03-15	58923.61	95.11	—	22.67±0.39	22.27±0.31	22.05±0.45	21.99±0.43	21.88±0.13	TNT

**Table 2.** Log of spectroscopic observations of SN 2019wep. The phase is measured with respect to  $V$ -max ( $\text{MJD}_{\text{max}}=58828.5$ ).

Phase	Telescope	Instrument	Range Å
-2.9	2.0m LJT	YFOSC	3400-7600
-2.9	2.0m LJT	YFOSC	3400-7600
-2.0	2.0m FTN	FLOYDS spectrograph	3400-9500
-1.0	2.0m FTN	FLOYDS spectrograph	3400-9500
0.0	2.0m FTN	FLOYDS spectrograph	3400-9700
1.4	2.0m LJT	YFOSC	3400-7600
5.0	2.0m FTN	FLOYDS spectrograph	3400-9700
7.2	2.0m LJT	YFOSC	3400-7600
8.0	2.0m FTN	FLOYDS spectrograph	3400-9500
12.3	2.0m LJT	YFOSC	3400-7600
13.0	2.0m FTN	FLOYDS spectrograph	3400-9500
18.3	2.0m LJT	YFOSC	3400-7600

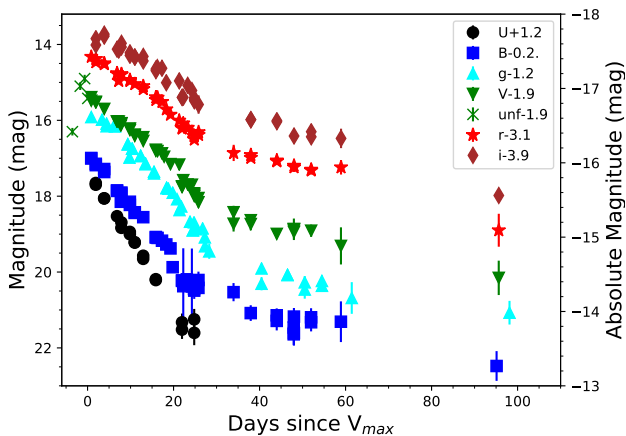


**Figure 1.**  $UBgVri/unfiltered$  light curve evolution of SN 2019wep.

$18.18 \pm 0.95$  mag and  $M_i = -17.98 \pm 0.99$  mag. The error on the peak magnitude is estimated from the estimated error on the peak date, the standard errors on the slope and intercept, and the slope-intercept covariance of the fit. We want to remark that the extrapolated peak only provides a limit on the magnitudes, and thus large error bars are associated with the estimation.

The rise time of an object is generally estimated as the difference between the estimated explosion epoch and the maximum. In the case of SN 2019wep we estimate the rise time to be  $4 \pm 3$  days. The error in rise time is the error in the explosion epoch and the epoch of

maximum propagated in quadrature. The rise time of SN 2019wep indicates that it is one of the fast-rising members among the SNe Iibn subclass and has a good match with SN 1999cq (cf. Table 4; Hosseinzadeh et al. 2017; Matheson et al. 2000).

The  $r$ -band light curve of SN 2019wep, between 0–30 days post maximum, has a decay rate of  $0.088 \pm 0.002$  mag  $\text{d}^{-1}$ . The  $V$  and  $i$ -band light curves follow approximately the same decline rate as  $r$ -band and roughly comparable to the SNe Iibn sample, i.e.,  $0.1$  mag  $\text{d}^{-1}$ , of course with few exceptions (Hosseinzadeh et al. 2017). The  $g$ - and  $B$ -band light curves decay slightly faster with a rate of  $\sim 0.145 \pm 0.003$  mag  $\text{d}^{-1}$ . Given the peak luminosity and decline rate, SN 2019wep also seems to follow the peak luminosity-decline rate relation of SNe Iibn proposed by Wang et al. (2021) concluding that more luminous SNe tend to have slower post-peak decline rates because of different CSM configurations.

Fast transients are the group of objects that rise and fade in brightness on timescales much shorter than those of other SNe (Drout et al. 2014; Arcavi et al. 2016; Pellegrino et al. 2021; Maeda & Moriya 2022). Their progenitor systems are uncertain and they have a featureless blue continuum similar to most SNe Iibn. The fast transients were an underrepresented class with a very few known examples (Ofek et al. 2010; Kasliwal et al. 2010) that were discovered by chance and displayed diverse observational properties. The recent high cadence surveys Pursiainen et al. (2018); Tampo et al. (2020); Andreoni et al. (2021) have allowed for a systematic search of fast transients. Using the ZTF sample, Ho et al. (2021) distinguished fast transients into three categories - i) sub-luminous SN Iib/Ic population, ii) luminous SN Iibn population, and iii) fast and blue optical transients (FBOTs). These studies have shown similarities between SNe Iibn and fast transients that are mostly powered by ejecta interacting with He-rich CSM. Moreover, SNe Iibn and fast transients show similar rise times, peak luminosity and decay rates (Clark et al. 2020; Xiang et al. 2021). Motivated with their similarity, we compare the absolute magnitude light curves of SN 2019wep in different bands with a sample of SNe Iibn (Hosseinzadeh et al. 2017) and fast transients (Drout et al. 2014) in the top and bottom panels respectively of Figure 2. The comparison sample has well covered peaks in  $g$ ,  $r$ ,  $i$ -bands which is missed in SN 2019wep. The only peak coverage in SN 2019wep is in the  $V$ -band. We plot the  $V$ -band absolute magnitude along with  $r$ -band in the top middle-panel (Figure 2) to show the comparison in peak magnitudes. The limiting peak absolute magnitudes of SN 2019wep in the  $r$  and  $i$ -bands are estimated by performing a linear fit as mentioned previously. We

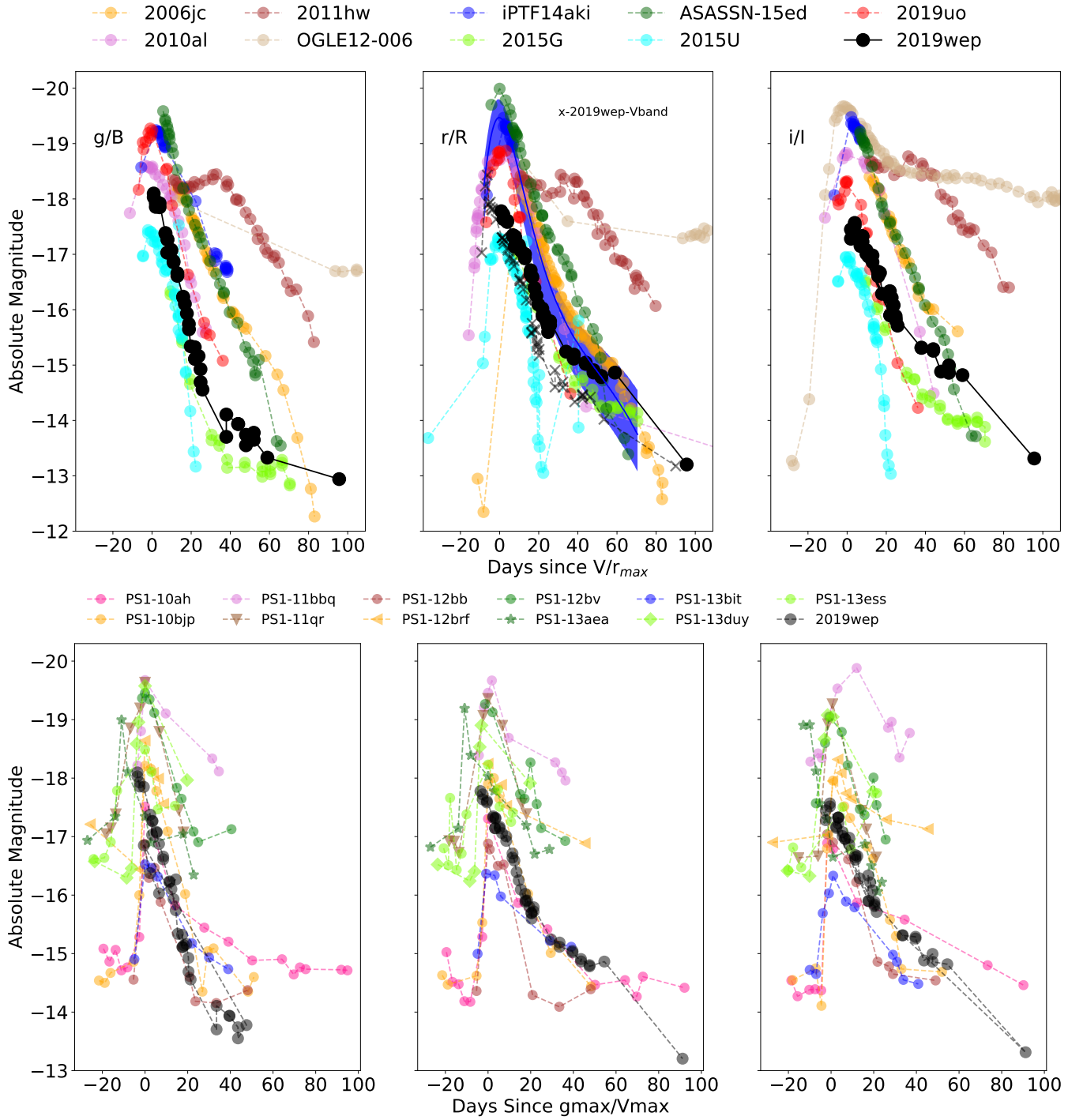


**Figure 2.**  $gri$  light curve comparisons of SN 2019wep with a sample of SNe Ibn (Hosseinzadeh et al. 2017) on the top three panels and with a group of fast transients in the bottom three panels taken from Drout et al. (2014). The SNe Ibn comparison sample includes SNe 2006jc (Pastorello et al. 2007; Foley et al. 2007), 2010al (Pastorello et al. 2015c), OGLE-SN-006 (Pastorello et al. 2015a), 2011hw (Pastorello et al. 2015c), iPTF14aki (Hosseinzadeh et al. 2017), 2015U (Shivvers et al. 2016; Hosseinzadeh et al. 2017), 2015G (Hosseinzadeh et al. 2017), ASASSN-15ed (Pastorello et al. 2015d) and 2019uo (Gangopadhyay et al. 2020a). Phase is plotted with respect to maxima for all the panels.

also estimate the 0–30 days decay rates of the sample of fast transients and find that it typically lies between 0.03–1 mag d<sup>-1</sup>. This indicates that the SN 2019wep light curves evolve faster than a prototypical SN II i.e. a SNe IIP/III with a post plateau decay rate of 0.01 mag d<sup>-1</sup> (Lyman et al. 2016; Bose et al. 2018), but has a evolution consistent with the categorised fast transients and lies at the faster decay end of SNe Ibn.

The top middle panel of Figure 2 also shows the normalized light curve of SNe Ibn (taken from Hosseinzadeh et al. (2017); comprising 95% of the SNe Ibn data) by the blue shaded region in the  $r$ -band. The normalized light curve was generated by first normalizing all light curves by their estimated peak magnitudes and using a Gaussian process to estimate the average light curve. We see that the light curve shape of SN 2019wep is well matched with that of SNe 2010al, 2019uo and ASASSN-15ed and the brightness is comparable to iPTF14aki. The estimated peak magnitude in SN 2019wep is towards the lower brightness limit of the SNe Ibn sample. Since non-detections were not included in generating the normalized light curve by Hosseinzadeh et al. (2017), the template is biased toward a brighter and shallower evolution at early times with longer rise times of SNe Ibn. In comparison to the fast transients, SN 2019wep lies at an average brightness. The light curve shape matches well with one of the fast transient PS1-10ah.

Figure 3 shows the correlation plots of SNe Ibn and fast transients where the  $\Delta_{m_{15}}$  and absolute magnitude are plotted against the rise time. The plot indicates that the rise time of SN 2019wep is shorter (even though large error bars are associated with these estimations) with respect to the rise time estimates of other SNe Ibn. The rise time of SN 2019wep is slightly larger than the average value of the fast transients. The  $\Delta_{m_{15}}$  value matches well with SN 1999cq and is lower as compared to other SNe Ibn. Even though rise times indicate that SN 2019wep lies in the faster end of the SNe Ibn sample, still, we remark that the light curves do not evolve faster than the group of fast transients. SN 2019wep is fainter than most of the SNe Ibn whereas it is of average brightness with respect to the fast transients.

We also compare the  $B - R/r$  color evolution of SN 2019wep with a number of SNe Ibn, which usually show heterogeneity in their color evolution (bottom plot; Figure 4). We see that SN 2019wep shows a color evolution similar to SNe 2010al, ASASSN-15ed and 2019uo in early times but later on transitions to blue. The  $B - r$  color of SN 2019wep increases up to 1.58 mag in  $\sim 52$  days post maximum, and subsequently becomes blue at  $\sim 93$  days. SN 2019wep continues to become redder for a longer duration of time than other SNe Ibn.

For, SNe 2010al, iPTF14aki, 2019uo, ASASSN-15ed and 2019wep the  $B - r$  color increases up to  $\sim 1$  mag,  $\sim 40$  days post maximum. At similar epochs, the color evolution of SN 2006jc was extremely blue ( $-0.5$  mag). The transition to the redder colours for SNe 2019wep indicates that it shows the characteristic of not a typical Ibn SN, but the one which shows a close resemblance to a SN Ib with time. This is in good agreement with the P cygni spectroscopic features that transition from narrow to broad, indicating a He-rich circumstellar shell around the progenitor star along with optically thick CSM. The late redder colors for SN 2006jc (Pastorello et al. 2007) and OGLE-2012-SN-006 (Pastorello et al. 2015a) are indicative of dust formation.

To construct the bolometric light curve of SN 2019wep between UV to IR bands, we used the SuperBol code (Nicholl 2018). The missing UV and NIR data was supplemented by extrapolating the Spectral Energy Distributions (SEDs) using the blackbody approximation and direct integration method as described in Lusk & Baron (2017). A linear extrapolation was performed in the UV regime at late times. The estimated limiting peak bolometric luminosity of SN 2019wep is  $8.8 \times 10^{42}$  erg s<sup>-1</sup> (top panel; Figure 4). The bolometric light curves of other SNe Ibn are also shown in the Figure. The overall light curve of SN 2019wep matches well with that of SN 2019uo (peak luminosity  $\sim 8.9 \times 10^{42}$  erg s<sup>-1</sup>). Gangopadhyay et al. (2020a) inferred that SN 2019uo was best described with a <sup>56</sup>Ni + CSM model which can be assumed to be consistent with SN 2019wep (given that both SNe have similar peak luminosities) with a <sup>56</sup>Ni mass of  $\sim 0.01_{-0.002}^{+0.003} M_{\odot}$ .

The bolometric light curve modelling of SN 2019wep has been performed in the work by Pellegrino et al. (2021) which we briefly summarise in this section. The physical parameters were derived from a best-fit hybrid model using the MINIM code (Chatzopoulos et al. 2013), which finds self-similar solutions to the propagation of forward and reverse shocks generated by the interaction between the SN ejecta and optically thick CSM as described by Chevalier (1982). The CSM has as its free parameters an inner radius  $R_{\text{ej}}$ , mass  $M_{\text{CSM}}$ , and density  $\rho_{\text{CSM}}$ , which has an assumed power law form with index  $n = 12$  in the outer region, and  $n = 0$  in the inner region. In addition to the CSM interaction, radioactive decay of <sup>56</sup>Ni is used as an additional luminosity source. Constant optical and gamma-ray opacities are also assumed.

Pellegrino et al. (2021) find that the bolometric evolution of SN 2019wep can be well explained by CSM interaction plus radioactive decay, following the mechanism by Chatzopoulos et al. (2013). The best-fit model

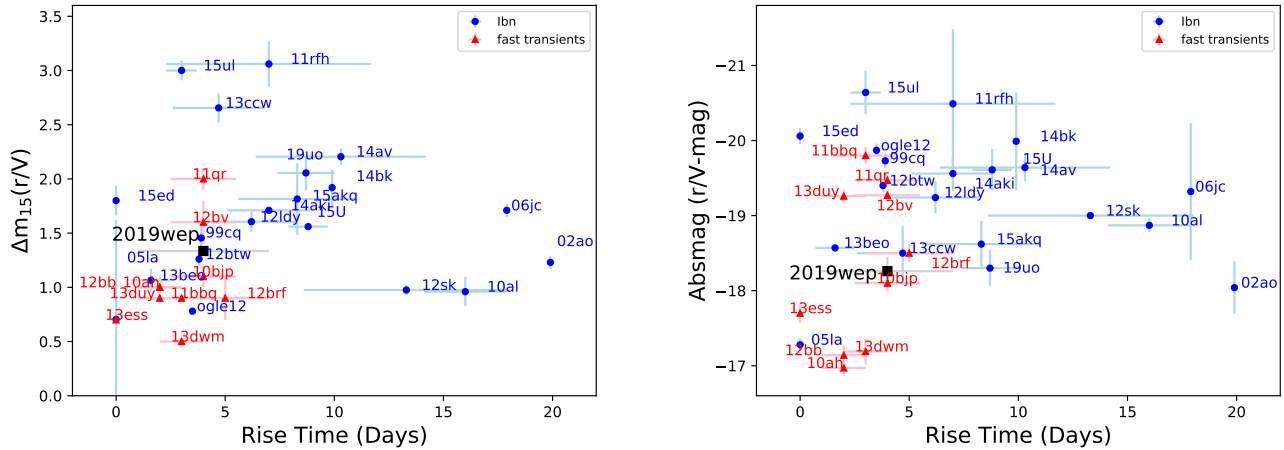


**Figure 3.** The  $\Delta m_{15}$  vs rise time (left panel) and absolute magnitude vs rise time (right panel) correlation plots of SN 2019wep with a sample of SNe Ibn and fast transients. The sample of type SNe Ibn has been taken from Hosseinzadeh et al. (2017); Gangopadhyay et al. (2020a) and the sample of fast transients are taken from Drout et al. (2014)

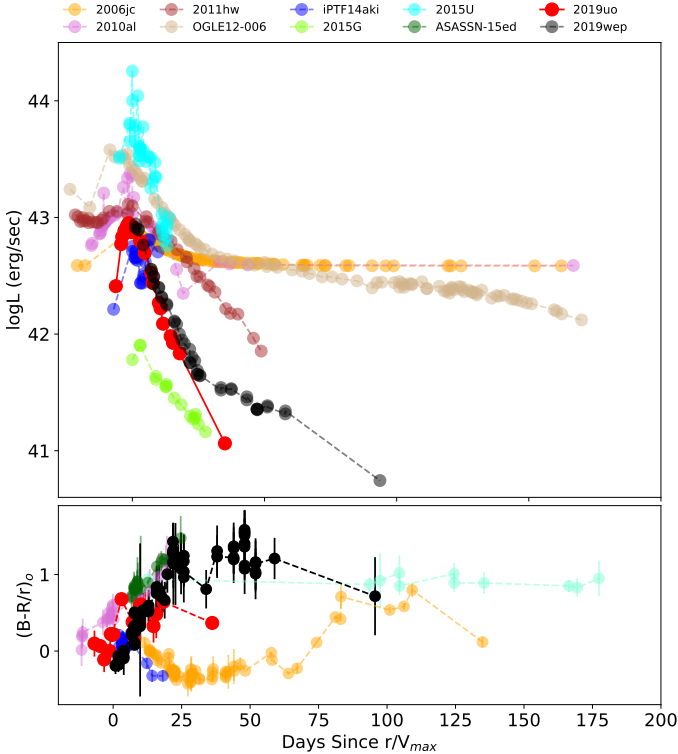


**Figure 4.** Complete bolometric light curve and  $B - R/r_0$  colour curve of SN 2019wep. The comparison sample includes SNe 2006jc (Pastorello et al. 2007; Foley et al. 2007), 2010al (Pastorello et al. 2015c), OGLE-SN-006 (Pastorello et al. 2015a), 2011hw (Pastorello et al. 2015c), iPTF14aki (Hosseinzadeh et al. 2017), 2015U (Shivvers et al. 2016; Hosseinzadeh et al. 2017), 2015G (Hosseinzadeh et al. 2017), ASASSN-15ed (Pastorello et al. 2015d) and 2019uo (Gangopadhyay et al. 2020a).

light curve to the data is shown in their Figure 1, with model parameters listed in their Table 6 (Pellegrino et al. 2021). This model has very similar CSM and ejecta parameters to that of SN 2019uo, including values of  $R_{ej}$ , ejecta mass  $M_{ej}$ ,  $M_{CSM}$ ,  $^{56}\text{Ni}$  mass  $M_{\text{Ni}}$ , and  $\rho_{CSM}$  that are consistent with one another. The best-fit parameters of SN 2019uo from Chatzopoulos et al. (2013) differ from those presented in Gangopadhyay et al. (2020a) due to the fact that different assumptions were made between the models used in these two studies, including assumed CSM density power law indices. Nevertheless, the inferred parameters for these two SNe Ibn indicate that they likely share similar CSM and explosion properties which was expected because both members belong to P cygni class of SNe Ibn with flash ionized features. A direct comparison of SNe Ibn with SNe Ib is not possible because of the difference in the luminosity powering mechanism. We see, however, that even though the obtained  $^{56}\text{Ni}$  masses are lower than the canonical SESNE (Maeda & Moriya 2022), the ejecta masses obtained are consistent with many SNe Ib as deciphered from the statistical analysis of Lyman et al. (2016); Prentice et al. (2016). This is also seen in the histograms (Figure 5) that compares SNe 2019uo and 2019wep with the statistical sample of SNe Ib taken from Prentice et al. (2019) and Taddia et al. (2018). We see that both SNe 2019uo and 2019wep lie at the lower limit of  $^{56}\text{Ni}$  mass while the ejecta masses are quite consistent with the sample. So, we can expect the appearance of P cygni spectroscopic features and broadening of the features with time. Also, since our obtained light curves are consistent with other SNe Ibn, the ejecta properties are expected to be within



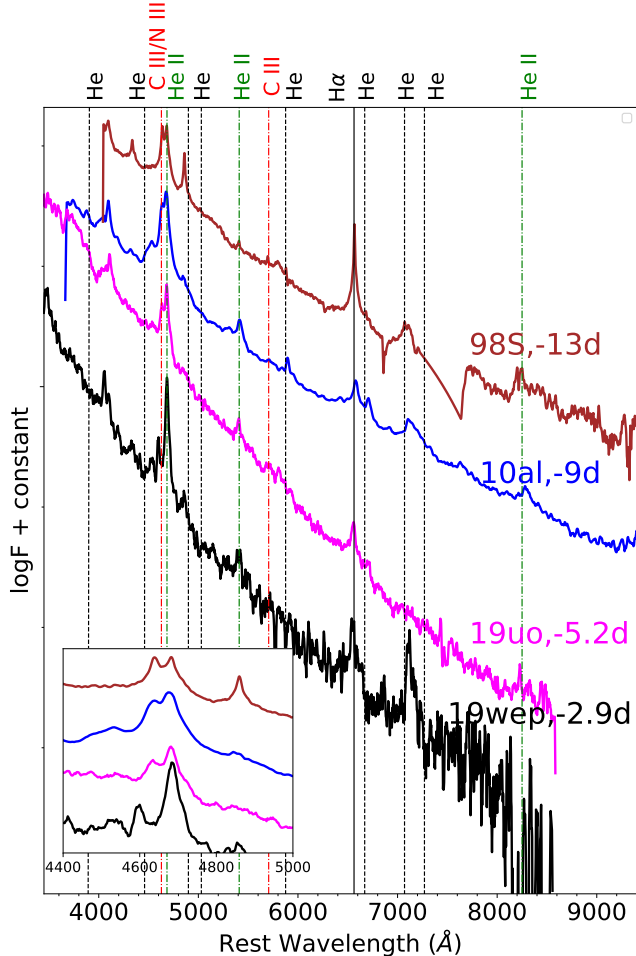


**Figure 7.** Spectral comparison of SN 2019wep at  $-2.9$  days with SNe 1998S (Fassia et al. 2001) 2010al (Pastorello et al. 2015c) and 2019uo (Gangopadhyay et al. 2020a). Prominent flash ionization features are marked.

SNe 2010al and 2019uo with a distinct blue continuum. The presence of this blue continuum also makes it similar to fast transients (Drout et al. 2014; Pellegrino et al. 2021). We fit a blackbody on the first three spectra ( $-2.9$ ,  $-2.0$  and  $-1.0$  day) of SN 2019wep which show that the photospheric temperature varies between 22,000 K to 15,000 K. However, we want to remark that the SEDs of these SNe peak in the UV regime (Drout et al. 2014) and the temperature will essentially depend on the UV brightness of the object. As such, the temperature derived from the photometry is uncertain owing to the lack of UV observations. A narrow  $H\alpha$  emission is seen in the early spectrum of SN 2019wep with a velocity of  $\sim 3000$  km  $\text{sec}^{-1}$  which is most likely due to interstellar gas in the host galaxy and some contribution from SN which we will explain in detail in later sections. We see typical features of emission in SN 2019wep around

$\sim 4660$  Å in the first five spectra ( $-2.9$  to 0.0 days). The emission components are double-peaked with two distinct transitions, the blue component peaking at 4643 Å and the red component peaking at 4682 Å. The red component at 4682 Å is due to He II at 4686 Å, whereas the blue component arises from a blend of C III 4648 Å and N III 4640 Å. A very weak, less prominent doubly ionized C III feature at 5696 Å is also seen. These signatures are interpreted as He rich signatures in a flash ionised CSM (Gal-Yam 2014; Pastorello et al. 2015b). Previously flash ionisation signatures of C III were seen in PTF12ldy and iPTF15ul (Hosseinzadeh et al. 2017). In SNe Ibn 2010al and 2019uo the flash ionization signatures of both C III and He II, typical of SNe II, are seen. Presence of such lines indicate that they could likely be originated from WR winds (Cooke et al. 2010; Silverman et al. 2010). Flash ionized signatures were previously noted in SNe IIn (e.g., SN 1998S; Fassia et al. (2001) and SN 2008fq; Taddia et al. (2013)). Groh (2014) reverted the WR progenitor scenario through the estimation of the physical parameters of a SN IIB 2013cu and found that the progenitor is not a WR star even though the flash ionized features showed WR like lines. A He II 5411 Å feature with a velocity between 1413 km  $\text{s}^{-1}$ –1483 km  $\text{s}^{-1}$  is also seen in the very early spectra ( $-2.9$ –0.0 day) of SN 2019wep. In the early spectra, an absorption feature is seen close to  $\sim 4000$  Å which is most likely due to the presence of O II and He II features, respectively.

Figure 7 shows a comparison of the early spectra of SNe 1998S (type IIn), 2010al (type Ibn) and 2019uo (type Ibn) with SN 2019wep. It is interesting to note that SN 2019wep shows the strongest flash features in the early spectrum as compared with other SNe Ibn. The spectrum of SN 2010al shows only C III features around 4650 Å, SN 2019wep shows C III features around 4650 Å and at 5696 Å in agreement with SN 2019uo. The inset in Figure 7 highlights these features, which also indicates that SN 2019wep shows the most significant He II feature.

As the SN evolves further (0.0 days), we see a distinct He I P cygni feature that is superimposed on a broader base (the continuum is not flat). The flash ionization spectral signatures vanishes with time and disappears on 1.4 days. From 5.0–18.3 days, features of Ca II, Si II, and Na ID also start developing (see Figure 6). Figure 8 shows the spectral comparison of SN 2019wep with other SNe Ibn in the phase range between 3 day to 10 day post maximum. At similar phases, the He I 5876 Å feature of SN 2019wep is similar to that identified in SN 2010al and SN 2019uo with a narrow P cygni feature while other members show a prominent emission

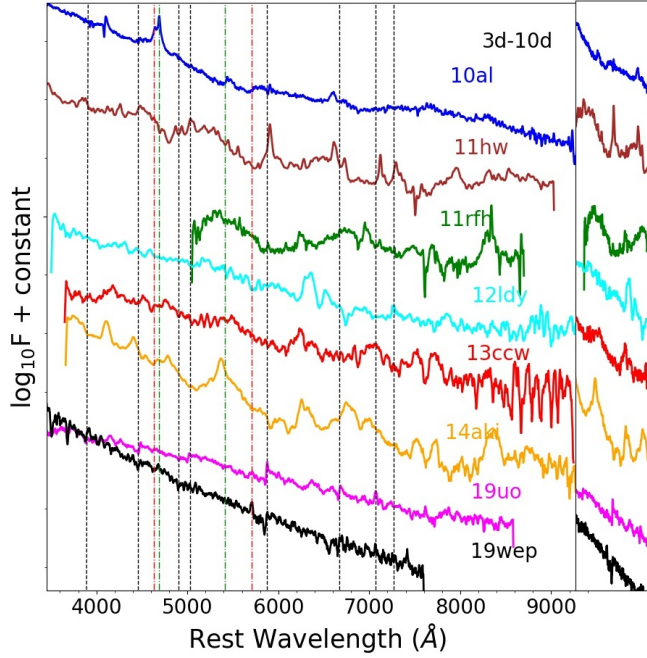


**Figure 8.** Comparison of the spectrum of SN 2019wep to other SNe Ibn. SN 2019wep belongs to the P cygni subclass and shows a close resemblance to SNe 2010al and 2019uo. The data for this are taken from — SNe 2010al (Pastorello et al. 2015b), 2011hw (Pastorello et al. 2015b), PTF11rfh (Hosseinzadeh et al. 2017), PTF12ldy (Hosseinzadeh et al. 2017), LSQ13ccw (Pastorello et al. 2015c), iPTF14aki (Hosseinzadeh et al. 2017) and 2019uo (Gangopadhyay et al. 2020a). The right panel of the plot shows the P cygni and the emission lines of He I 5876 Å feature.

profile. Also, the continuum of SN 2019wep is bluer as compared to all other SNe of the comparison sample. However, the He I P cygni feature of SN 2019wep is broader than SNe 2010al and 2019uo, and is superimposed over a broader emission line. On the other hand, the He I P cygni profile in SN 2010al is over a flat continuum. The flash ionization signatures in SN 2019wep have vanished in this phase, but in SN 2010al these signatures are still visible. The spectral signatures of SN 2019wep (specially He I as shown in zoomed version in the right inset) indicates that SN 2019wep belongs to the “P cygni” subclass.

We see distinct broad emission lines of He I developing from 7.2–18.3 day indicating similarity to a SN Ib. For a more evident comparison, we plot the spectrum of SN 2019wep in Figure 9 with SN Ibn ASASSN-15ed (Pastorello et al. 2015d) and a few prototypical SNe Ib between 15–20 days after maximum. A comparison of the He I velocity of SN 2019wep shows that it has a typical absorption FWHM velocity of  $\sim 5000 \pm 1000$  km sec<sup>-1</sup>. At similar epochs, the FWHM velocity of

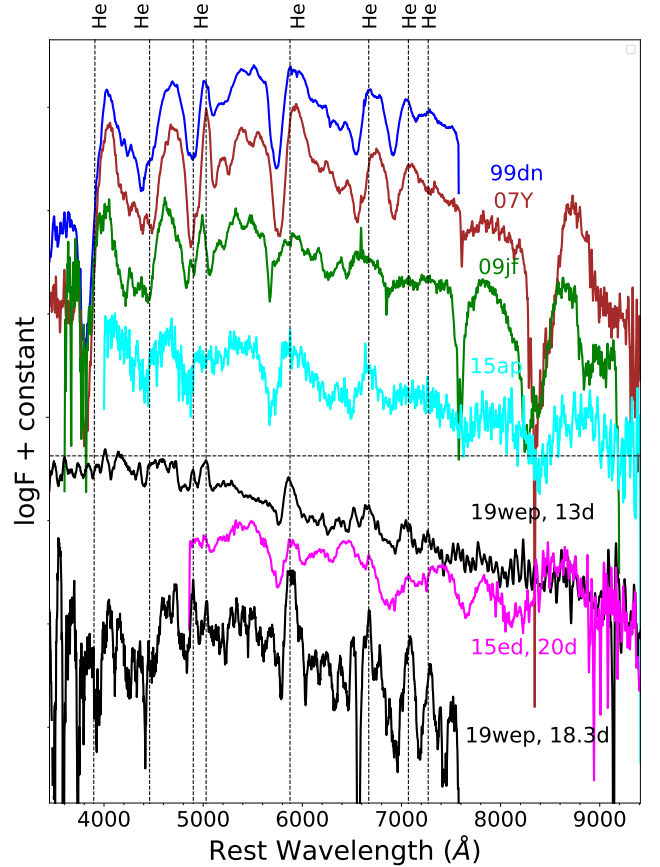


**Figure 9.** Comparison of the spectrum of SN 2019wep to other SN Ib and a transitioning SN Ibn ASASSN-15ed. The data are taken from - ASASSN-15ed (Pastorello et al. 2015d), SNe- 1999dn (Benetti et al. 2011), 2007Y (Stritzinger et al. 2009), 2009jf (Valenti et al. 2011) and 2015ap (Gangopadhyay et al. 2020b).

ASASSN-15ed is  $6300 \pm 1000$  km sec<sup>-1</sup> which is comparable to that of SN 2019wep. This is less than the typical SN Ib velocity of our comparison sample which has absorption trough velocity between 7000–9000 km sec<sup>-1</sup>. The major difference observed between SNe Ibn and SNe Ib spectra is that SNe Ibn have more symmetric profiles, while in SNe Ib the absorption dominates over the emission. Additionally, the absorption components of He I in SN 2019wep are almost similar to SNe Ib spectra suggesting a higher kinetic energy per mass unit in the SN ejecta, specially in the late phases of SNe Ibn that develop broad lines (Pastorello et al. 2015d). The simultaneous presence of a very narrow feature at early phases and transitioning to broad features suggests that these features arise from different emitting regions: the broader He I P cygni features are likely a signature of the SN ejecta, while the narrow He I P cygni lines are generated in the unperturbed, He-rich CSM. At early

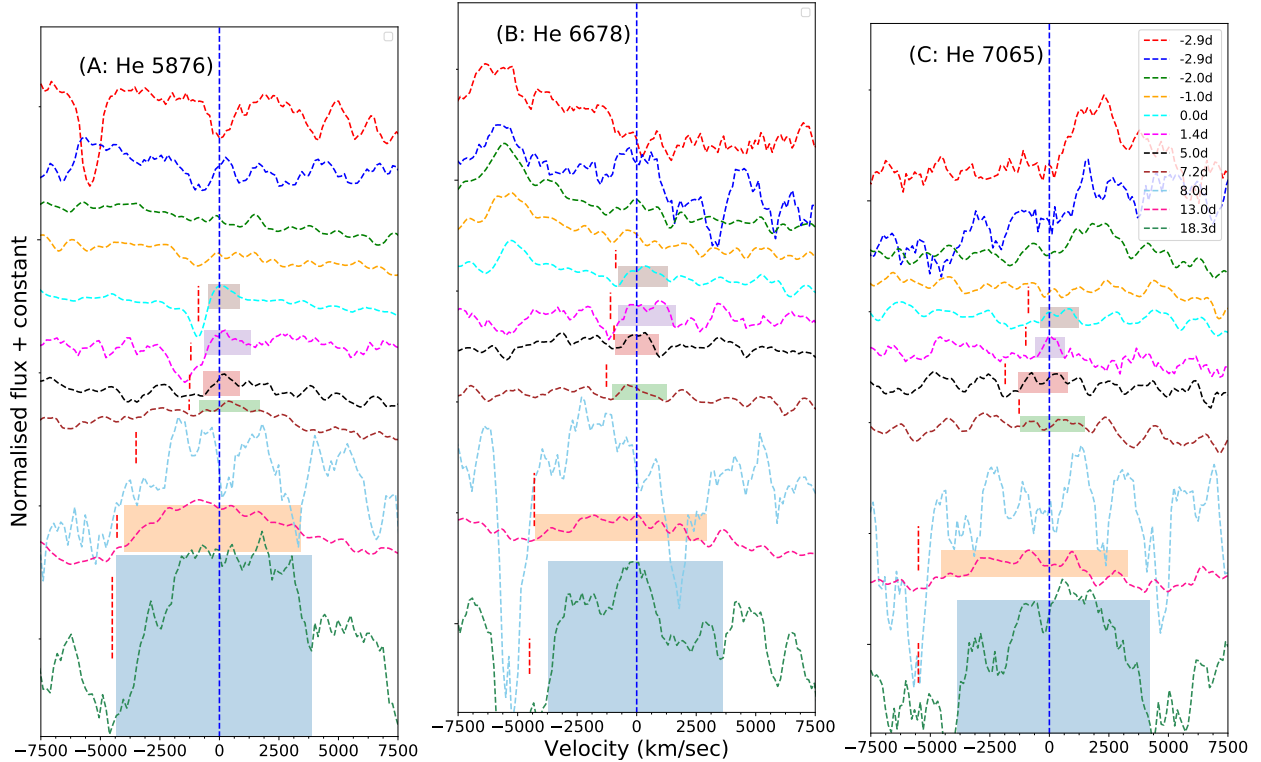


**Figure 10.** Line evolution of He I 5876, 6678 and 7065 Å. These lines broaden with time showing prominent evolution. The blue dotted line corresponds to the central velocity of 0 km sec<sup>-1</sup>. The red dotted line represents the absorption minima corresponding to the velocity estimations. The shaded regions in the plot describes the area used for the estimation of the equivalent widths.

phases, the narrow lines are formed in the photosphere located in a dense shell. This shell is either continuously photoionized by early ejecta-CSM interaction in the inner CSM regions and/or by the initial shock breakout. Once recombination occurs, the shell becomes transparent and we see the signatures of underlying SN ejecta and the spectrum is dominated by broad P cygni lines.

Figure 10 shows the evolution of He I 5876, 6676, 7065 Å feature in the velocity space. We see a narrow P cygni profile which gradually evolves with time and shows a broad emission on top. The physical explanation behind the origin of the “P cygni” subclass could be a shell of He around the progenitor star surrounded by a dense CSM. As the optically thick shell is lit by the explosion, the narrow P cygni features transition to broader emission as the shell is swept up by the SN ejecta. The viewing angle dependence could also affect this scenario; if the CSM is asymmetric and, we have a He rich torus, then P cygni features would only be visible if the system is viewed edge-on, while emission features can be seen only if it is viewed face-on. On the contrary, [Karamehmetoglu et al. \(2019\)](#) suggest that dominance of emission at late phases is not because of being optically thin, but because they lack other lines to branch into it. UV and

X-ray emission arising at the shock boundary are the source of He ionisation and recombination. The ionised region outside the shock leads to electron scattering and emission, P cygni features usually originate from optical depths  $\leq 1$ . X-rays penetrating further into the P cygni producing regions will fill in the absorption and lead to emission features. Thus, this provides an alternative scenario to the transitioning of P cygni to emission features of He I lines for SNe Ibn. Asymmetric CSM, thus, plays an important role in the origin of these unusual features. Much of the ejecta usually moves undisturbed by the prevalent CSM configuration. Luminosity generation as a consequence of the interaction of the equatorial CSM beneath the photosphere continues, but, spectral signatures remain hidden until the photosphere recedes. This is the primary cause driving the blue continuum at early stages followed by the appearance of broadened redshifted He features ([Andrews & Smith 2018](#)).

We measure the expansion velocities and equivalent widths (EWs) of three neutral He lines (5876, 6678, and 7065 Å), wherever visible. The emission lines of He I were fit using a Gaussian on a linear continuum. The estimation of EW involves calculation of the integral of the flux normalized to the local continuum. We do

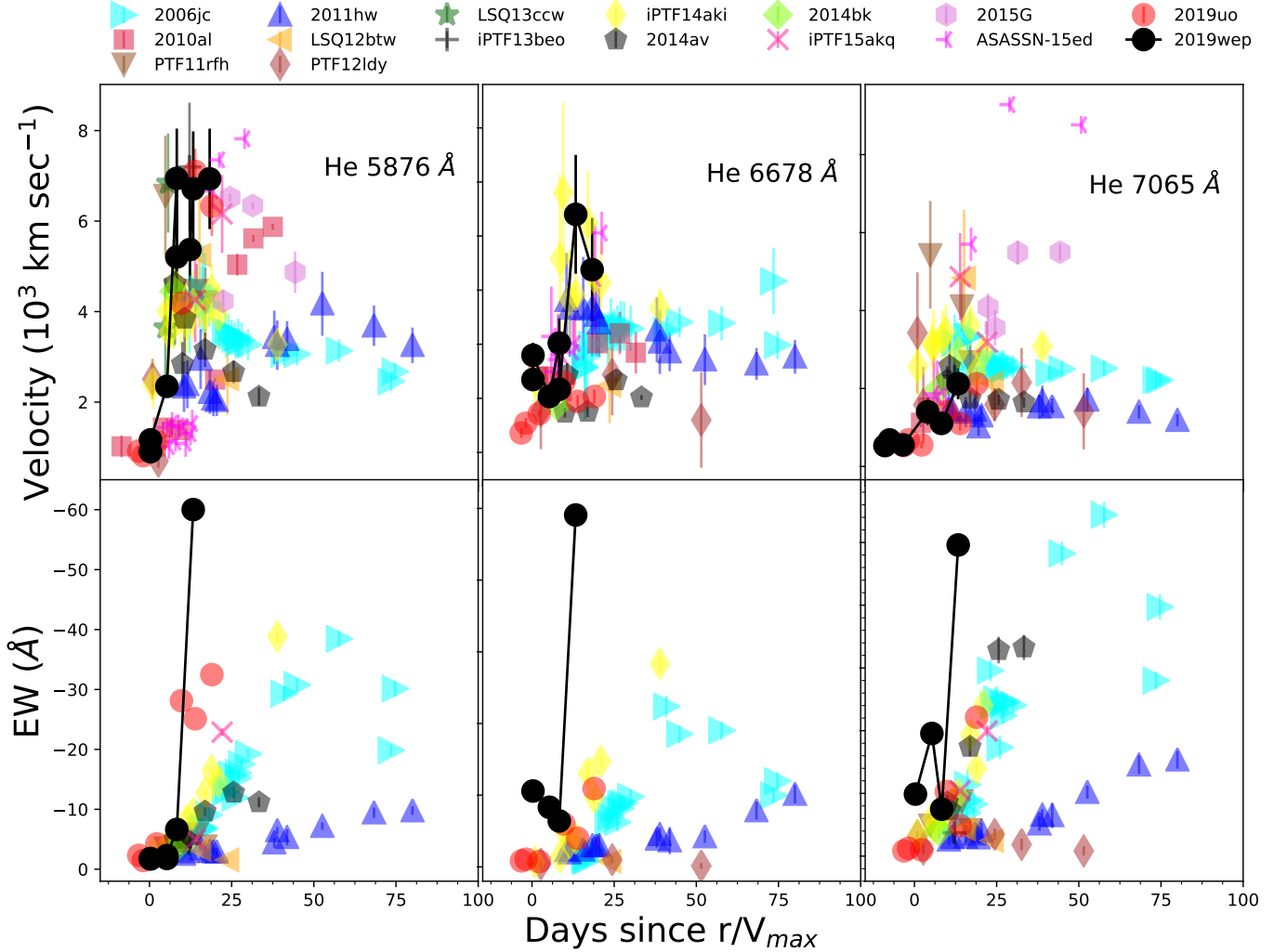


**Figure 11.** Evolution of line velocities and equivalent widths of He I emission lines is shown in top and bottom panels, respectively. The data for this are taken from — SNe 2006jc (Foley et al. 2007; Pastorello et al. 2008a), 2010al (Pastorello et al. 2015b), 2011hw (Pastorello et al. 2015b), PTF11rfrh (Hossein-zadeh et al. 2017), LSQ12btw (Pastorello et al. 2015c), OGLE12-006 (Pastorello et al. 2015a), PTF12ldy (Hossein-zadeh et al. 2017), iPTF13beo (Gorbikov et al. 2014), LSQ13ccw (Pastorello et al. 2015c), iPTF14aki (Hossein-zadeh et al. 2017), 2014av (Pastorello et al. 2016), 2014bk (Pastorello et al. 2016), iPTF15akq (Hossein-zadeh et al. 2017), ASASSN-15ed (Pastorello et al. 2015d), 2015G (Hossein-zadeh et al. 2017) and 2019uo (Gangopadhyay et al. 2020a).

not measure the EW of the P cygni lines. The velocities reported are estimated from the absorption minima of P cygni profiles. Figure 11 shows the evolution of velocity and EW for a sample of SNe I<sub>bn</sub> taken from Hossein-zadeh et al. (2017). We see an increasing trend in both the line velocities and EW of the He lines. The velocity estimates of SN 2019wep lie at the upper range of SNe I<sub>bn</sub> and show a faster evolution. In SN 2019wep, the broad features seen are more prominent than typical emission velocity of SNe I<sub>bn</sub> around maxima varying between 6000-8000 km sec<sup>-1</sup> (Hossein-zadeh et al. 2017). SN 2019wep has a good resemblance with ASASSN-15ed reaching broader emission profiles as seen in the

P cygni subclass (Hossein-zadeh et al. 2017) while the emission subclass shows less evolution in line velocities. The EWs of the absorption component of He I lines for SN 2019wep are at an extreme high end than the normal SNe I<sub>bn</sub>. This is also an indication that perhaps SN 2019wep lies somewhere between SN Ib and SNe I<sub>bn</sub>.

#### He I line velocity evolution :

A wide diversity and heterogeneity is observed in the spectral evolution of SNe I<sub>bn</sub> in accordance with SNe II<sub>n</sub>. The physical parameters of SNe I<sub>bn</sub> strongly depend on the composition, geometry, mass and density

profile of CSM along with the residual stellar envelope at the time of explosion.

The properties of stellar wind and CSM can be inferred probing the line emitting regions. Spectra of interacting SNe IIn and SNe Ibn are typically produced in different gas regions (Chevalier & Fransson 1985; Chugai 1997). The emitting material moving at different velocities are indicated by different components of SNe with varying widths. The slow expanding, photoionised CSM is usually indicated by narrow emission lines (with velocities from a few hundreds to  $6500 \text{ km sec}^{-1}$ ). This gas is unshocked CSM produced by the progenitor star before exploding as a SN. This gives information on the mass-loss history of the SN progenitors. When a clear P cygni profile is identified, the position of the core of the blue-shifted absorption gives an idea of the expanding material. When this component is not detected, the velocity is estimated through the FWHM of the strongest He I emission lines, obtained after deblending the full line profile with Gaussian fits. Figure 12 shows the He I velocity of SN 2019wep, estimated from the weighted average of first two days to be  $510 \pm 20 \text{ km sec}^{-1}$ . The expected range of WR wind speeds ( $500\text{-}3200 \text{ km sec}^{-1}$ ) (Crowther & Smartt 2007) is shown as the purple shaded region, the expected wind speeds of LBV stars ( $50\text{-}600 \text{ km sec}^{-1}$ ) (Smith 2017) is shown in red and the expected wind speed range of RSG stars ( $10\text{-}50 \text{ km sec}^{-1}$ ) (van Loon et al. 2005) shown in black. Objects like SN 2019wep which show low CSM velocity are well-matched with other low velocity SNe 2011hw ( $200\text{-}250 \text{ km sec}^{-1}$ ) and 2005la (about  $500 \text{ km sec}^{-1}$ ). For such SNe, an  $H\alpha$  line of moderate strength is also found to be associated with the SNe. Scenarios of H lines along with modest stellar wind velocities (a few hundreds  $\text{km sec}^{-1}$ ) are compatible with stellar progenitors which are transitioning between the LBV and the Wolf-Rayet (WNE-type) stages (Pastorello et al. 2008b, 2015e, 2016). PS1-12sk is one such event which showed narrow He I lines and relatively weak intermediate-width  $H\alpha$  lines and is uniquely associated with an elliptical galaxy. The plot also shows that the velocity of He I, represented by horizontal bars, lies at the lower end of the velocity distribution of SNe Ibn.

The traditional description by Humphreys & Davidson (1994) defines LBVs as single stars between  $60\text{-}100 M_{\odot}$  at a transitional phase in the evolution of the most massive stars, between the main-sequence O-type stars and the H-deficient WR stars. However, Smith & Tombleson (2015) found that the LBVs are surprisingly isolated from O-type stars. Smith & Tombleson (2015) further claimed that many LBVs are likely to be the product of binary evolution and cannot drive the mass-

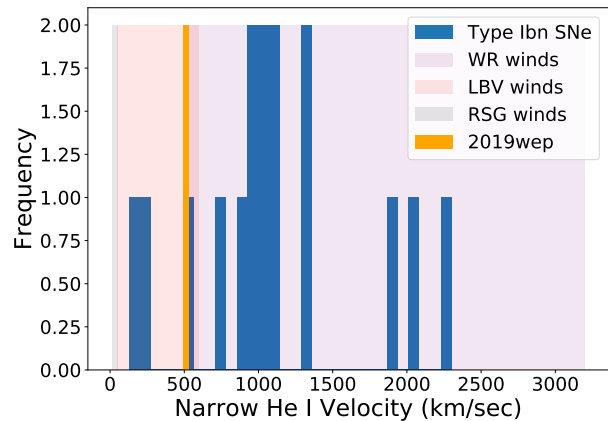


**Figure 12.** Histogram representing the sample of SNe Ibn taken from Pastorello et al. (2016) with blue bars. The orange shaded bar is the velocity with errors of SN 2019wep averaged over the first two days. The black, red and purple shaded regions represent the wind speeds of RSG, LBV and WR stars respectively.

loss mechanism leading to WR phase. Humphreys et al. (2016) again reverted the scenario proposed by Smith & Tombleson (2015) highlighting their uneven sample and reconfirm that LBVs are evolved massive stars that have shed a lot of mass and are moving towards WR phase.

Following the above description both single and binary progenitor scenario are equally likely in case of SN 2019wep with the progenitor having a reminiscent  $H\alpha$  feature typical of LBV stars and gradually transitioning to a WR phase having a dense CSM owing to the mass-loss rates of the LBV. It has been established that the sites of SNe Ibn are generally associated with star-forming environments (Pastorello et al. 2015b), with one exceptional case where no/little association of star-formation activity was found (PS1-12sk, Sanders et al. 2013; Hosseinzadeh et al. 2019). Thus, the popular and speculative progenitors are typically single massive WR stars with mass  $\geq 18 M_{\odot}$  (Tominaga et al. 2008; Maeda & Moriya 2022) or a binary progenitor scenario which may be equally likely (Foley et al. 2007).

### Origin of $H\alpha$ feature:

The  $H\alpha$  feature originating in SNe serve as an important classifier among the interacting SNe group. Although narrow He I emission lines are frequently detected in the spectra of SNe IIn, the relative strengths between  $H\alpha$  and the most prominent optical lines He I ( $5876$  and  $7065 \text{ \AA}$ ) determines the classification of the transient as a SN IIn, SN Ibn or even a transitional object between these two SN types.

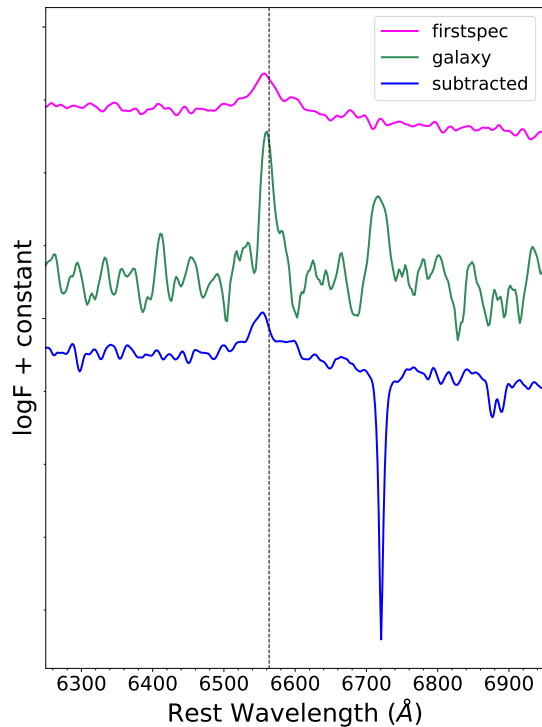


**Figure 13.** The first day, galaxy and subtracted spectra of SN 2019wep taken with the LCO networks. A reminiscent  $H\alpha$  is seen in the subtracted profile.

In the two transitional SNe IIn/Ibn 2005la and 2011hw, Balmer lines were prominently detected (Pastorello et al. 2008b, 2015e, 2016). The strength of  $H\alpha$  feature in both these SNe are comparable with He I lines. In the early spectrum of SN 2005la (Modjaz et al. 2014),  $H\alpha$  showed a narrow, marginally resolved ( $\text{FWHM} \sim 400 \text{ km sec}^{-1}$ ) component, superposed on a broader base with a P cygni profile while the highest resolution spectrum of SN 2011hw (Pastorello et al. 2015e) showed an unresolved  $H\alpha$  ( $\text{FWHM} \leq 250 \text{ km sec}^{-1}$ ) observed over a much broader wing and the intermediate  $H\alpha$  component with  $\text{FWHM}$  monotonically increasing between  $1350 \text{ km sec}^{-1}$  and  $2350 \text{ km sec}^{-1}$ . However, most of the SNe Ibn show no prominent  $H\alpha$  lines or, in some cases, the identification of  $H\alpha$  is controversial. For example, the detection of multiple lines of C II in the spectra of PS1-12sk (Sanders et al. 2013) argued - at least in the case of that object - against the identification of H lines.

We also see little  $H\alpha$  at early time in SN 2019wep. To check whether the  $H\alpha$  is from the host galaxy or is a reminiscent contribution from the SN, we obtained a

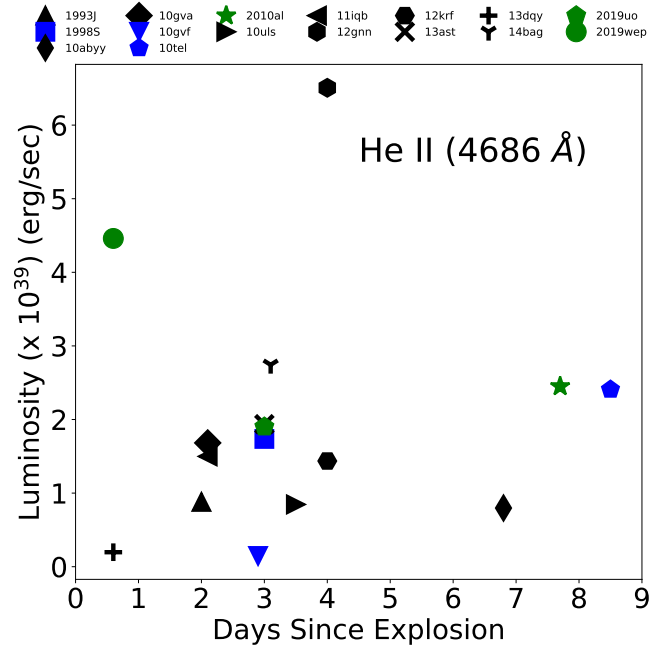


**Figure 14.** He II 4686 Å luminosity and equivalent width of a sample of SNe showing flash ionization features in their early spectra with SNe II in black, IIn in blue, and Ibn in green (Khazov et al. 2016; Gangopadhyay et al. 2020a). SN 2019wep is shown as a green circle.

spectrum in June 2021 from 2.0m FTM. This was used as a host galaxy template for subtraction on the first spectrum of the SN obtained with the same instrumental setup. The flux of the  $H\alpha$  feature was matched. The subtracted spectrum is shown in Figure 13. Even after spectral subtraction, we see a residual  $H\alpha$  component with  $\text{FWHM} \sim 1050 \text{ km sec}^{-1}$ . When comparing with the first LCO spectrum, it looks like that one also had a broad  $H\alpha$  base, not present in the host spectrum. So, we propose that at least some (and perhaps all) of the narrow  $H\alpha$  seen is from the host, but we cannot rule out that some of it (especially because there's a broad base) is from the SN. We, however, concur that there may be a contamination due to C II. In terms of spectroscopic properties, a transitioning behaviour like SN 2011hw is noticed for SN 2019wep.

To ascertain the origin of SNe Ibn, a sample of 13 SNe II from literature (including SNe IIb, IIP and IIn; Khazov et al. (2016)) and Ibn (Hosseinzadeh et al. 2017; Gangopadhyay et al. 2020a), with flash ionisation signatures within 10 days of explosion, are collected. The H lines are usually contaminated by host galaxy lines, we therefore select the relatively isolated and unblended He II 4686 Å line. Since the He II lines are much narrower than the lines from the SN ejecta, they can serve as a good tool to probe the flash-ionized CSM. While

measuring the luminosities, we remove the continuum by fitting a linear function. Figure 14 shows the typical luminosity of the He II line in SN 2019wep and other SNe II/IIn/Ibn. From the figure we see that only one SN along with SN 2019wep has been detected very early post explosion for which flash ionization signatures are detected owing to the recombination of CSM. The average luminosity of He II for SN 2019wep is higher than almost all other SNe II, IIn and Ibn which is indicative of the fact that the amount of CSM in SN 2019wep is larger than average SNe II, IIn and Ibn sample at early time. This highlights the need for high cadence SN spectroscopy at very early phase to detect signatures of flash ionisation which are also indicative of presence of CSM and will in turn be useful to infer the possible progenitors.

## 5. SUMMARY

The paper summarises the photometric and spectroscopic evolution of the SN Ibn 2019wep from  $-0.4$  to 95 days post maximum. The availability of early data points in TNS were useful to constrain the  $V$ -band maxima. The light curve decline is slower than the fast transients but is consistent with the SNe Ibn group with a typical decay rate of  $\sim 0.1 \text{ mag d}^{-1}$  (Hosseinzadeh et al. 2017). Fast transients are one of the exciting findings with characteristic timescales of  $\leq 10$  days, missed in most of the traditional surveys either due to poor resolution of the spectrum or unavailability of follow-up spectroscopic observations. A recent study by Ho et al. (2021) classified SNe Ibn as a subclass of fast transients due to their very similar rise times and blue continuum. This study motivated us to compare the properties of SN 2019wep with samples of SNe Ibn and fast transients. The limits on the absolute magnitude ( $M_V = -18.26 \pm 0.20 \text{ mag}$  and  $M_r = -18.18 \pm 0.95$ ) shows that the SN lies at the fainter end of SN Ibn subclass but is closer to the average absolute magnitude of the fast transients.

The correlation plots also suggest that the rise time of SN 2019wep is higher than that of the fast transients but is shorter than the average SNe Ibn value. Our analysis suggests that SN 2019wep decays fast and has low luminosity in comparison to other SNe Ibn. We quote the results of the bolometric light curve modelling of SN 2019wep from Pellegrino et al. (2021). The bolometric light curve of SN 2019wep has striking resemblance with SN 2019uo suggesting a comparable  $^{56}\text{Ni}$  mass in both SNe. The ejecta mass of SN 2019wep is consistent with SNe Ib samples, even though the models cannot be directly comparable because of different physical mechanisms involved. The low  $^{56}\text{Ni}$  mass of SN 2019wep may suggest a significant fallback in the center which can

also possibly explain the consistency of the ejecta mass of SN 2019wep with SNe Ib sample. The color evolution of SN 2019wep is unique, placing it between SNe Ib and SNe Ibn. The spectroscopic features of SN 2019wep indicate that it is one of the rare SNe Ibn with signatures of flash ionisation. The early, prominent flash ionisation lines of He II, C III, and N III are detected in the spectra, similar to SN 2019uo and SN 2010al. The disappearance of narrow He I features immediately after maximum and the transitioning to broad P cygni He I features hints towards a lateral shift from SN Ibn to SN Ib group. We interpret that the resemblance to SN Ib is due to the fact that the SN ejecta that is likely hidden by the CSM interaction becomes evident when the recombination comes into play at late phases. The P cygni subclass most likely originates from a He-rich shell around the progenitor surrounded by a dense CSM, or it may be due to viewing angle dependency. Asymmetry of the CSM configuration also plays a major role in this aspect. This is also validated by the equivalent widths of He I features. The estimated line velocities are lower than the average values of SNe Ibn, but they show a faster evolution as compared to the ‘‘emission’’ subclass. The low He I velocity of CSM and the presence of residual  $H\alpha$  in the spectroscopic features indicate that SN 2019wep is a transitional SN Ibn with progenitor scenario lying between a LBV and a WR star. Maeda & Moriya (2022) essentially found that the progenitor of SNe Ibn are WR stars with mass  $\geq 18 M_\odot$ . While Ho et al. (2021) estimate that the volumetric rate of SNe Ibn population is 0.5% of CCSNe, Maeda & Moriya (2022) with their updated estimations found that the volumetric rates is 1% of CCSNe population. This is of course below the fraction of SNe Ibn with masses  $\geq 18 M_\odot$  but many of them are undetected in optical because of emission of large fraction of UV radiation for these candidate SNe (Maeda & Moriya 2022). High cadence UV surveys are thus, quintessential to detect ‘UV Ibn’ SNe population.

## ACKNOWLEDGMENTS

We thank the referee for several critical comments and useful suggestions which has improved the presentation of the paper. We thank the support of the staff of the Xinglong 2.16 m and Lijiang 2.4 m telescope, for their support during observations. This work was partially supported by the Open Project Program of the Key Lab-

oratory of Optical Astronomy, National Astronomical Observatories, Chinese Academy of Sciences. Funding for the Lijiang 2.4 m telescope has been provided by Chinese Academy of Sciences and the People’s Government of Yunnan Province. We acknowledge Weizmann Interactive Supernova data REPOSITORY (WISeREP; <http://wiserep.weizmann.ac.il>). DAH acknowledges support from NSF grant AST-1313404. The work of XW is supported by the National Science Foundation of China (NSFC grants 12033003, 11633002, and 11761141001), the Major State Basic Research Development Program (grant 2016YFA0400803), and the Scholar Program of Beijing Academy of Science and Technology (DZ:BS202002). This work makes use of data obtained with the LCO Network. KM acknowledges BRICS grant DST/IMRCD/BRICS/Pilotcall/ProFCheap/2017(G) and the DST/JSPS grant, DST/INT/JSPS/P/281/2018

for the present work. IA is a CIFAR Azrieli Global Scholar in the Gravity and the Extreme Universe Program and acknowledges support from that program, from the European Research Council (ERC) under the European Union’s Horizon 2020 research and innovation program (grant agreement number 852097), from the Israel Science Foundation (grant number 2752/19), from the United States - Israel Binational Science Foundation (BSF), and from the Israeli Council for Higher Education Alon Fellowship. JZ is supported by the NSFC (grants 12173082, 11773067), by the Youth Innovation Promotion Association of the CAS (grants 2018081), and by the Ten Thousand Talents Program of Yunnan for Top-notch Young Talents. The LCO team is supported by NSF grants AST-1911151 and AST-1911225.

*Software:* `lcogtspipe` (Valenti et al. 2011, 2016), IRAF (Tody 1986, 1993), DAOPHOT (Stetson 1987), HOTPANTS (Becker 2015), `superbol` (Lusk 2016)

## REFERENCES

- Andreoni, I., Coughlin, M. W., Kool, E. C., et al. 2021, *ApJ*, 918, 63, doi: [10.3847/1538-4357/ac0bc7](https://doi.org/10.3847/1538-4357/ac0bc7)
- Andrews, J. E., & Smith, N. 2018, *MNRAS*, 477, 74, doi: [10.1093/mnras/sty584](https://doi.org/10.1093/mnras/sty584)
- Arcavi, I., Wolf, W. M., Howell, D. A., et al. 2016, *ApJ*, 819, 35, doi: [10.3847/0004-637X/819/1/35](https://doi.org/10.3847/0004-637X/819/1/35)
- Becker, A. 2015, HOTPANTS: High Order Transform of PSF AND Template Subtraction. <http://ascl.net/1504.004>
- Bellm, E. 2014, in *The Third Hot-wiring the Transient Universe Workshop*, ed. P. R. Wozniak, M. J. Graham, A. A. Mahabal, & R. Seaman, 27–33. <https://arxiv.org/abs/1410.8185>
- Bellm, E. C., Kulkarni, S. R., Barlow, T., et al. 2019, *PASP*, 131, 068003, doi: [10.1088/1538-3873/ab0c2a](https://doi.org/10.1088/1538-3873/ab0c2a)
- Benetti, S., Turatto, M., Valenti, S., et al. 2011, *MNRAS*, 411, 2726, doi: [10.1111/j.1365-2966.2010.17873.x](https://doi.org/10.1111/j.1365-2966.2010.17873.x)
- Bose, S., Dong, S., Kochanek, C. S., et al. 2018, *ApJ*, 862, 107, doi: [10.3847/1538-4357/aacb35](https://doi.org/10.3847/1538-4357/aacb35)
- Chatzopoulos, E., Wheeler, J. C., & Couch, S. M. 2013, *ApJ*, 776, 129, doi: [10.1088/0004-637X/776/2/129](https://doi.org/10.1088/0004-637X/776/2/129)
- Chevalier, R. A. 1982, *ApJL*, 259, L85, doi: [10.1086/183853](https://doi.org/10.1086/183853)
- Chevalier, R. A., & Fransson, C. 1985, *Supernova Interaction with a Circumstellar Wind and the Distance to SN 1979c*, ed. N. Bartel, Vol. 224, 123, doi: [10.1007/3-540-15206-7\\_53](https://doi.org/10.1007/3-540-15206-7_53)
- Chugai, N. N. 1997, *Ap&SS*, 252, 225, doi: [10.1023/A:1000847125928](https://doi.org/10.1023/A:1000847125928)
- Clark, P., Maguire, K., Innes, C., et al. 2020, *MNRAS*, 492, 2208, doi: [10.1093/mnras/stz3598](https://doi.org/10.1093/mnras/stz3598)
- Cooke, J., Ellis, R. S., Nugent, P. E., et al. 2010, *The Astronomer’s Telegram*, 2491, 1
- Crowther, P., & Smartt, S. 2007, *Astronomy and Geophysics*, 48, 1.35, doi: [10.1111/j.1468-4004.2007.48135.x](https://doi.org/10.1111/j.1468-4004.2007.48135.x)
- Drout, M. R., Chornock, R., Soderberg, A. M., et al. 2014, *ApJ*, 794, 23, doi: [10.1088/0004-637X/794/1/23](https://doi.org/10.1088/0004-637X/794/1/23)
- Fassia, A., Meikle, W. P. S., Chugai, N., et al. 2001, *MNRAS*, 325, 907, doi: [10.1046/j.1365-8711.2001.04282.x](https://doi.org/10.1046/j.1365-8711.2001.04282.x)
- Foley, R. J., Smith, N., Ganeshalingam, M., et al. 2007, *ApJL*, 657, L105, doi: [10.1086/513145](https://doi.org/10.1086/513145)
- Gal-Yam, A. 2014, in *American Astronomical Society Meeting Abstracts*, Vol. 223, American Astronomical Society Meeting Abstracts #223, 235.02
- Gal-Yam, A. 2019, *ApJ*, 882, 102, doi: [10.3847/1538-4357/ab2f79](https://doi.org/10.3847/1538-4357/ab2f79)
- Gal-Yam, A., & Leonard, D. C. 2009, *Nature*, 458, 865, doi: [10.1038/nature07934](https://doi.org/10.1038/nature07934)
- Gal-Yam, A., Arcavi, I., Ofek, E. O., et al. 2014, *Nature*, 509, 471, doi: [10.1038/nature13304](https://doi.org/10.1038/nature13304)
- Gal-Yam, A., Bruch, R., Schulze, S., et al. 2022, *Nature*, 601, 201, doi: [10.1038/s41586-021-04155-1](https://doi.org/10.1038/s41586-021-04155-1)
- Gangopadhyay, A., Misra, K., Hiramatsu, D., et al. 2020a, *ApJ*, 889, 170, doi: [10.3847/1538-4357/ab6328](https://doi.org/10.3847/1538-4357/ab6328)
- Gangopadhyay, A., Misra, K., Sahu, D. K., et al. 2020b, *MNRAS*, 497, 3770, doi: [10.1093/mnras/staa1821](https://doi.org/10.1093/mnras/staa1821)

- Gorbikov, E., Gal-Yam, A., Ofek, E. O., et al. 2014, *MNRAS*, 443, 671, doi: [10.1093/mnras/stu1184](https://doi.org/10.1093/mnras/stu1184)
- Groh, J. H. 2014, *A&A*, 572, L11, doi: [10.1051/0004-6361/201424852](https://doi.org/10.1051/0004-6361/201424852)
- Ho, A. Y. Q., Perley, D. A., Gal-Yam, A., et al. 2021, arXiv e-prints, arXiv:2105.08811. <https://arxiv.org/abs/2105.08811>
- Hosseinzadeh, G., McCully, C., Zabludoff, A. I., et al. 2019, *ApJL*, 871, L9, doi: [10.3847/2041-8213/aafc61](https://doi.org/10.3847/2041-8213/aafc61)
- Hosseinzadeh, G., Arcavi, I., Valenti, S., et al. 2017, *ApJ*, 836, 158, doi: [10.3847/1538-4357/836/2/158](https://doi.org/10.3847/1538-4357/836/2/158)
- Huang, F., Li, J.-Z., Wang, X.-F., et al. 2012, *Research in Astronomy and Astrophysics*, 12, 1585, doi: [10.1088/1674-4527/12/11/012](https://doi.org/10.1088/1674-4527/12/11/012)
- Humphreys, R. M., & Davidson, K. 1994, *PASP*, 106, 1025, doi: [10.1086/133478](https://doi.org/10.1086/133478)
- Humphreys, R. M., Weis, K., Davidson, K., & Gordon, M. S. 2016, *ApJ*, 825, 64, doi: [10.3847/0004-637X/825/1/64](https://doi.org/10.3847/0004-637X/825/1/64)
- Karamehmetoglu, E., Fransson, C., Sollerman, J., et al. 2019, arXiv e-prints, arXiv:1910.06016. <https://arxiv.org/abs/1910.06016>
- Kasliwal, M. M., Kulkarni, S. R., Gal-Yam, A., et al. 2010, *ApJL*, 723, L98, doi: [10.1088/2041-8205/723/1/L98](https://doi.org/10.1088/2041-8205/723/1/L98)
- Khazov, D., Yaron, O., Gal-Yam, A., et al. 2016, *ApJ*, 818, 3, doi: [10.3847/0004-637X/818/1/3](https://doi.org/10.3847/0004-637X/818/1/3)
- Lusk, J. A. 2016, SuperBoL: Module for calculating the bolometric luminosities of supernovae. <http://ascl.net/1609.019>
- Lusk, J. A., & Baron, E. 2017, *PASP*, 129, 044202, doi: [10.1088/1538-3873/aa5e49](https://doi.org/10.1088/1538-3873/aa5e49)
- Lyman, J. D., Bersier, D., James, P. A., et al. 2016, *MNRAS*, 457, 328, doi: [10.1093/mnras/stv2983](https://doi.org/10.1093/mnras/stv2983)
- Maeda, K., & Moriya, T. J. 2022, arXiv e-prints, arXiv:2201.00955. <https://arxiv.org/abs/2201.00955>
- Mao, X., Gao, W., Ding, Y., Zhang, M., & Gao, X. 2019, *Transient Name Server Discovery Report*, 2019-2556, 1
- Matheson, T., Filippenko, A. V., Chornock, R., Leonard, D. C., & Li, W. 2000, *AJ*, 119, 2303, doi: [10.1086/301352](https://doi.org/10.1086/301352)
- Modjaz, M., Blondin, S., Kirshner, R. P., et al. 2014, *AJ*, 147, 99, doi: [10.1088/0004-6256/147/5/99](https://doi.org/10.1088/0004-6256/147/5/99)
- Moriya, T. J., & Maeda, K. 2016, *ApJ*, 824, 100, doi: [10.3847/0004-637X/824/2/100](https://doi.org/10.3847/0004-637X/824/2/100)
- Morozova, V., Piro, A. L., & Valenti, S. 2017, *ApJ*, 838, 28, doi: [10.3847/1538-4357/aa6251](https://doi.org/10.3847/1538-4357/aa6251)
- Munari, U., & Zwitter, T. 1997, *A&A*, 318, 269
- Nicholl, M. 2018, *Research Notes of the American Astronomical Society*, 2, 230, doi: [10.3847/2515-5172/aaf799](https://doi.org/10.3847/2515-5172/aaf799)
- Nyholm, A., Sollerman, J., Tartaglia, L., et al. 2020, *A&A*, 637, A73, doi: [10.1051/0004-6361/201936097](https://doi.org/10.1051/0004-6361/201936097)
- Ofek, E. O., Rabinak, I., Neill, J. D., et al. 2010, *ApJ*, 724, 1396, doi: [10.1088/0004-637X/724/2/1396](https://doi.org/10.1088/0004-637X/724/2/1396)
- Pastorello, A., Smartt, S. J., Mattila, S., et al. 2007, *Nature*, 447, 829, doi: [10.1038/nature05825](https://doi.org/10.1038/nature05825)
- Pastorello, A., Mattila, S., Zampieri, L., et al. 2008a, *MNRAS*, 389, 113, doi: [10.1111/j.1365-2966.2008.13602.x](https://doi.org/10.1111/j.1365-2966.2008.13602.x)
- Pastorello, A., Quimby, R. M., Smartt, S. J., et al. 2008b, *MNRAS*, 389, 131, doi: [10.1111/j.1365-2966.2008.13603.x](https://doi.org/10.1111/j.1365-2966.2008.13603.x)
- Pastorello, A., Wyrzykowski, L., Valenti, S., et al. 2015a, *MNRAS*, 449, 1941, doi: [10.1093/mnras/stu2621](https://doi.org/10.1093/mnras/stu2621)
- Pastorello, A., Benetti, S., Brown, P. J., et al. 2015b, *MNRAS*, 449, 1921, doi: [10.1093/mnras/stu2745](https://doi.org/10.1093/mnras/stu2745)
- Pastorello, A., Hadjijska, E., Rabinowitz, D., et al. 2015c, *MNRAS*, 449, 1954, doi: [10.1093/mnras/stv335](https://doi.org/10.1093/mnras/stv335)
- Pastorello, A., Prieto, J. L., Elias-Rosa, N., et al. 2015d, *MNRAS*, 453, 3649, doi: [10.1093/mnras/stv1812](https://doi.org/10.1093/mnras/stv1812)
- Pastorello, A., Tartaglia, L., Elias-Rosa, N., et al. 2015e, *MNRAS*, 454, 4293, doi: [10.1093/mnras/stv2256](https://doi.org/10.1093/mnras/stv2256)
- Pastorello, A., Wang, X. F., Ciabattari, F., et al. 2016, *MNRAS*, 456, 853, doi: [10.1093/mnras/stv2634](https://doi.org/10.1093/mnras/stv2634)
- Pastorello, A., Vogl, C., Taubenberger, S., et al. 2021, *Transient Name Server AstroNote*, 71, 1
- Pellegrino, C., Howell, D. A., Vinkó, J., et al. 2021, arXiv e-prints, arXiv:2110.15370. <https://arxiv.org/abs/2110.15370>
- Perley, D. A., Sollerman, J., Schulze, S., et al. 2022, *ApJ*, 927, 180, doi: [10.3847/1538-4357/ac478e](https://doi.org/10.3847/1538-4357/ac478e)
- Poznanski, D., Prochaska, J. X., & Bloom, J. S. 2012, *MNRAS*, 426, 1465, doi: [10.1111/j.1365-2966.2012.21796.x](https://doi.org/10.1111/j.1365-2966.2012.21796.x)
- Prentice, S. J., Mazzali, P. A., Pian, E., et al. 2016, *MNRAS*, 458, 2973, doi: [10.1093/mnras/stw299](https://doi.org/10.1093/mnras/stw299)
- Prentice, S. J., Ashall, C., James, P. A., et al. 2019, *MNRAS*, 485, 1559, doi: [10.1093/mnras/sty3399](https://doi.org/10.1093/mnras/sty3399)
- Pursiainen, M., Childress, M., Smith, M., et al. 2018, *MNRAS*, 481, 894, doi: [10.1093/mnras/sty2309](https://doi.org/10.1093/mnras/sty2309)
- Sanders, N. E., Soderberg, A. M., Foley, R. J., et al. 2013, *ApJ*, 769, 39, doi: [10.1088/0004-637X/769/1/39](https://doi.org/10.1088/0004-637X/769/1/39)
- Schlafly, E. F., & Finkbeiner, D. P. 2011, *ApJ*, 737, 103, doi: [10.1088/0004-637X/737/2/103](https://doi.org/10.1088/0004-637X/737/2/103)
- Schlegel, E. M. 1990, *MNRAS*, 244, 269
- Shivvers, I., Zheng, W. K., Mauerhan, J., et al. 2016, *MNRAS*, 461, 3057, doi: [10.1093/mnras/stw1528](https://doi.org/10.1093/mnras/stw1528)
- Silverman, J. M., Kleiser, I. K. W., Morton, A. J. L., & Filippenko, A. V. 2010, *Central Bureau Electronic Telegrams*, 2223, 1

- Smith, N. 2017, *Interacting Supernovae: Types IIn and Ibn*, ed. A. W. Alsabti & P. Murdin, 403, doi: [10.1007/978-3-319-21846-5\\_38](https://doi.org/10.1007/978-3-319-21846-5_38)
- Smith, N., Chornock, R., Silverman, J. M., Filippenko, A. V., & Foley, R. J. 2010, *ApJ*, 709, 856, doi: [10.1088/0004-637X/709/2/856](https://doi.org/10.1088/0004-637X/709/2/856)
- Smith, N., Foley, R. J., & Filippenko, A. V. 2008, *ApJ*, 680, 568, doi: [10.1086/587860](https://doi.org/10.1086/587860)
- Smith, N., & Tombleson, R. 2015, *MNRAS*, 447, 598, doi: [10.1093/mnras/stu2430](https://doi.org/10.1093/mnras/stu2430)
- Stetson, P. B. 1987, *PASP*, 99, 191, doi: [10.1086/131977](https://doi.org/10.1086/131977)
- Stritzinger, M., Mazzali, P., Phillips, M. M., et al. 2009, *ApJ*, 696, 713, doi: [10.1088/0004-637X/696/1/713](https://doi.org/10.1088/0004-637X/696/1/713)
- Strotjohann, N. L., Ofek, E. O., Gal-Yam, A., et al. 2021, *ApJ*, 907, 99, doi: [10.3847/1538-4357/abd032](https://doi.org/10.3847/1538-4357/abd032)
- Sun, N.-C., Maund, J. R., Hirai, R., Crowther, P. A., & Podsiadlowski, P. 2020, *MNRAS*, 491, 6000, doi: [10.1093/mnras/stz3431](https://doi.org/10.1093/mnras/stz3431)
- Taddia, F., Stritzinger, M. D., Sollerman, J., et al. 2013, *A&A*, 555, A10, doi: [10.1051/0004-6361/201321180](https://doi.org/10.1051/0004-6361/201321180)
- Taddia, F., Stritzinger, M. D., Bersten, M., et al. 2018, *A&A*, 609, A136, doi: [10.1051/0004-6361/201730844](https://doi.org/10.1051/0004-6361/201730844)
- Tampo, Y., Tanaka, M., Maeda, K., et al. 2020, *ApJ*, 894, 27, doi: [10.3847/1538-4357/ab7ccc](https://doi.org/10.3847/1538-4357/ab7ccc)
- Tody, D. 1986, in *Society of Photo-Optical Instrumentation Engineers (SPIE) Conference Series*, Vol. 627, *Instrumentation in astronomy VI*, ed. D. L. Crawford, 733, doi: [10.1117/12.968154](https://doi.org/10.1117/12.968154)
- Tody, D. 1993, in *Astronomical Society of the Pacific Conference Series*, Vol. 52, *Astronomical Data Analysis Software and Systems II*, ed. R. J. Hanisch, R. J. V. Brissenden, & J. Barnes, 173
- Tominaga, N., Limongi, M., Suzuki, T., et al. 2008, *ApJ*, 687, 1208, doi: [10.1086/591782](https://doi.org/10.1086/591782)
- Valenti, S., Fraser, M., Benetti, S., et al. 2011, *MNRAS*, 416, 3138, doi: [10.1111/j.1365-2966.2011.19262.x](https://doi.org/10.1111/j.1365-2966.2011.19262.x)
- Valenti, S., Sand, D., Pastorello, A., et al. 2014, *MNRAS*, 438, L101, doi: [10.1093/mnrasl/slt171](https://doi.org/10.1093/mnrasl/slt171)
- Valenti, S., Howell, D. A., Stritzinger, M. D., et al. 2016, *MNRAS*, 459, 3939, doi: [10.1093/mnras/stw870](https://doi.org/10.1093/mnras/stw870)
- van Loon, J. T., Cioni, M. R. L., Zijlstra, A. A., & Loup, C. 2005, *A&A*, 438, 273, doi: [10.1051/0004-6361:20042555](https://doi.org/10.1051/0004-6361:20042555)
- Wang, S.-Q., & Li, L. 2019, arXiv e-prints, arXiv:1905.12623. <https://arxiv.org/abs/1905.12623>
- Wang, X., Lin, W., Zhang, J., et al. 2021, *ApJ*, 917, 97, doi: [10.3847/1538-4357/ac0c17](https://doi.org/10.3847/1538-4357/ac0c17)
- Xiang, D., Wang, X., Lin, W., et al. 2021, *ApJ*, 910, 42, doi: [10.3847/1538-4357/abdeba](https://doi.org/10.3847/1538-4357/abdeba)
- Zhang, J., Ye, K., & Wang, X. 2019a, *Transient Name Server Classification Report*, 2019-2565, 1
- . 2019b, *The Astronomer's Telegram*, 13337, 1